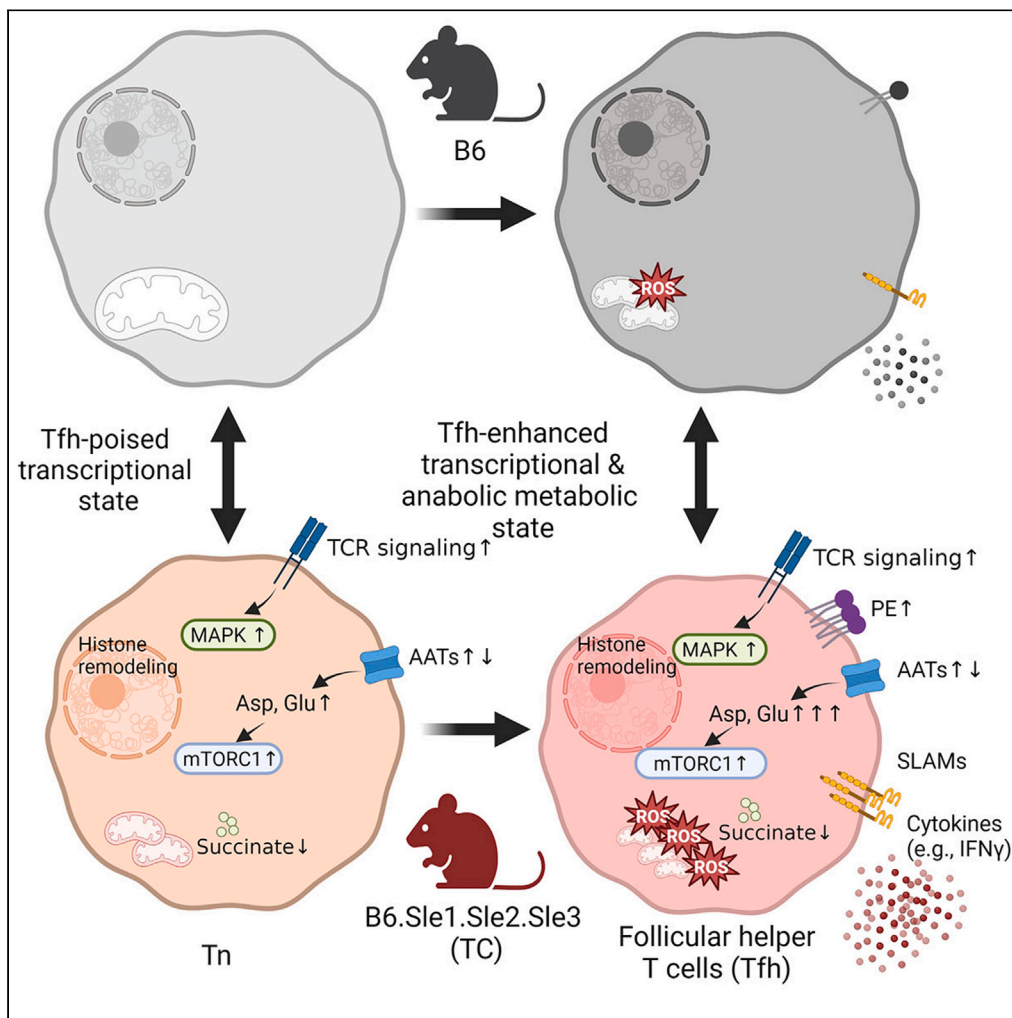


Article

Transcriptional and metabolic programs promote the expansion of follicular helper T cells in lupus-prone mice



Minghao Gong,  
Seung-Chul Choi,  
Yuk Pheel Park, ...,  
Jeffrey C.  
Rathmell, Mansour  
Mohamazadeh,  
Laurence Morel

morel@uthscsa.edu

Highlights

Lupus follicular T (Tfh) cells express a signaling and effector gene signature

This enhanced gene signature is initiated in naive CD4 T cells (Tn)

Lupus Tn and Tfh cells present altered mitochondrial functions

Amino acid metabolism and anabolic programs are altered in lupus Tfh cells



## Article

## Transcriptional and metabolic programs promote the expansion of follicular helper T cells in lupus-prone mice

Minghao Gong,<sup>1,4</sup> Seung-Chul Choi,<sup>2,4</sup> Yuk Pheel Park,<sup>2</sup> Xueyang Zou,<sup>1</sup> Ahmed S. Elshikha,<sup>1</sup> Valerie A. Gerriets,<sup>3</sup> Jeffrey C. Rathmell,<sup>3</sup> Mansour Mohamazadeh,<sup>2</sup> and Laurence Morel<sup>2,5,\*</sup>

## SUMMARY

**The expansion of follicular helper T (Tfh) cells, which is tightly associated with the development of lupus, is reversed by the inhibition of either glycolysis or glutaminolysis in mice. Here we analyzed the gene expression and metabolome of Tfh cells and naive CD4<sup>+</sup> T (Tn) cells in the B6.*Sle1.Sle2.Sle3* (triple congenic, TC) mouse model of lupus and its congenic B6 control. Lupus genetic susceptibility in TC mice drives a gene expression signature starting in Tn cells and expanding in Tfh cells with enhanced signaling and effector programs. Metabolically, TC Tn and Tfh cells showed multiple defective mitochondrial functions. TC Tfh cells also showed specific anabolic programs including enhanced glutamate metabolism, malate-aspartate shuttle, and ammonia recycling, as well as altered dynamics of amino acid content and their transporters. Thus, our study has revealed specific metabolic programs that can be targeted to specifically limit the expansion of pathogenic Tfh cells in lupus.**

## INTRODUCTION

Follicular helper T (Tfh) cells are a specialized subset of cluster of differentiation (CD) CD4<sup>+</sup> T cells that provide co-stimulatory signals to germinal center (GC) B cells to undergo class-switching, somatic hypermutation, and differentiation into long-lived plasma cells. Class-switched high-affinity autoantibodies are a major mediator of tissue damage in systemic lupus erythematosus (SLE). The frequency of Tfh cells is expanded in SLE patients proportionally with disease activity<sup>1–3</sup> and rises in SLE patients evaluated shortly after diagnosis.<sup>4</sup> A higher frequency of Tfh and GC B cells has been found in all mouse models of lupus, in which the pharmacologic or genetic targeting of interleukin (IL)-21, a cytokine specifically produced by Tfh cells, ameliorated disease.<sup>5,6</sup>

The molecular mechanisms responsible for Tfh cell differentiation and function have been well defined in response to a foreign antigen challenge.<sup>7,8</sup> However, the specific mechanisms that drive the spontaneous expansion of Tfh cells in lupus are largely unknown. To address this issue, we have used the B6.*Sle1.Sle2.Sle3* triple congenic (TC) mouse model, which carries the three NZM2410 susceptibility loci that are necessary and sufficient to develop lupus in a C57BL/6 (B6) background.<sup>9</sup> In this model, we have identified two genetic determinants in the *Sle1* locus, which contribute to Tfh cell expansion. The Pbx1-d dominant negative splice isoform of Pbx1 in the *Sle1a* susceptibility locus favors Tfh cell expansion at the expense of impaired regulatory T cells.<sup>10</sup> *Sle1b* corresponds to variants in a cluster of genes of the signaling lymphocytic activation molecule (SLAM) family,<sup>11</sup> which are known to regulate Tfh cell responses.<sup>12,13</sup> Among them, a different ratio of *Ly108* isoforms promotes the expansion of Tfh cells.<sup>14,15</sup>

The cellular metabolism of immune cells is altered in SLE patients and mouse models of the disease, and some of these alterations may offer therapeutic targets.<sup>16–18</sup> Specifically, we have shown that CD4<sup>+</sup> T cells from SLE patients and TC mice are more metabolically active, with a greater glycolysis and mitochondrial oxidative phosphorylation (OXPHOS). Reducing the metabolic activity of CD4<sup>+</sup> T cells with inhibitors of glycolysis and OXPHOS was therapeutic, implying that metabolism and effector function were causally linked in lupus CD4<sup>+</sup> T cells.<sup>19</sup> We have also shown that naive CD4<sup>+</sup> T cells from pre-autoimmune TC mice were more metabolically active than their B6 counterparts,<sup>19</sup> suggesting an intrinsic genetic alteration of TC CD4<sup>+</sup> T cells that was independent of autoimmune activation.

<sup>1</sup>Department of Pathology, Immunology, and Laboratory Medicine, University of Florida, Gainesville, FL 32610, USA

<sup>2</sup>Department of Microbiology, Immunology, and Molecular Genetics, University of Texas Health San Antonio, San Antonio, TX 78229, USA

<sup>3</sup>Vanderbilt Center for Immunobiology, Department of Pathology, Microbiology, and Immunology, Vanderbilt University Medical Center, Nashville, TN 37232, USA

<sup>4</sup>These authors contributed equally

<sup>5</sup>Lead contact

\*Correspondence: [morel@uthscsa.edu](mailto:morel@uthscsa.edu)

<https://doi.org/10.1016/j.isci.2023.106774>



Although the field of immunometabolism has exploded in the last decade, the metabolic programs that sustain Tfh cells have been relatively less studied.<sup>20</sup> Tfh cells are considered as metabolically quiescent,<sup>21,22</sup> but they require both mammalian target of rapamycin complex 1 and 2 (mTORC1 and mTORC2) signaling,<sup>23</sup> and their proliferation involves both glycolysis and oxidative phosphorylation.<sup>23,24</sup> We have shown that spontaneous Tfh cells were more glycolytic than naive CD4<sup>+</sup> T cells, and TC Tfh cells were more glycolytic than B6 Tfh cells.<sup>25</sup> Accordingly, treatment with 2-deoxy-D-glucose (2DG), a non-metabolizable glucose analogue that inhibits the first step of glycolysis, reduced the frequency of both Tfh and GC B cells and eliminated the production of autoantibodies in multiple models of lupus-prone mice. Remarkably, the 2DG treatment preferentially targeted spontaneously expanded Tfh cells in lupus-prone mice, which contained autoreactive specificities, but did not impair the frequency or function of Tfh cells induced by a viral or protein antigen challenge in either lupus or control mice. Consistent with this result, the deletion of the main glucose transporter, *Slc2a1*, in CD4<sup>+</sup> T cells did not impair Tfh cell differentiation in B6 mice; however, *Slc2a1* overexpression expanded Tfh cells in response to protein immunization.<sup>23</sup> Treatment of lupus or control mice with 6-diazo-5-oxo-L-norleucine (DON), an inhibitor of *Gls1*, the first enzyme in glutaminolysis, reduced the expression of B-cell lymphoma 6 (BCL-6), the Tfh cell master regulator, and eliminated both spontaneous and protein immunization-induced GCs in both lupus and control mice. *Gls1* deficiency in total CD4<sup>+</sup> T cells altered their Th1 and Th17 functions.<sup>26,27</sup> However, the impact of *Gls1* deletion on Tfh cell development has not been examined.

Tfh cells from lupus-prone TC mice have a transcriptional profile distinct from B6 controls.<sup>25</sup> The transcriptional signature of spontaneous Tfh cells was also different from that of Lymphocytic Choriomeningitis Virus (LCMV)-induced Tfh cells in the *Sle1.Yaa* lupus-prone mice.<sup>28</sup> The metabolic profile of Tfh cells has only been characterized comparatively to other effector subsets in *in vitro*-polarized cells from B6 mice.<sup>23</sup> The current study was performed to further characterize the transcriptomic signature of TC Tfh cells comparatively to B6 Tfh cells by including their naive T (Tn) cell counterparts. We also integrated metabolic profiling of both these subsets. Our results showed that lupus-susceptibility genes drive the expression of a specific gene signature that starts in Tn cells and expands in Tfh cells toward enhanced signaling and effector programs. Metabolically, TC Tfh cells showed profound defects in mitochondrial programs that may be at the root of their reliance on glycolysis. TC Tfh cells also showed specific anabolic programs with enhanced glutamate metabolism and malate-aspartate shuttle. Thus, our study has revealed specific metabolic programs that can be targeted to limit the expansion of pathogenic Tfh cells.

## RESULTS

### Spontaneous Tfh cells from TC lupus-prone mice express a robust transcriptional signature

Our previous microarray analysis demonstrated that PD1<sup>+</sup>CXCR5<sup>+</sup>CD4<sup>+</sup> Tfh cells isolated from TC mice carried a different transcriptional program as compared to B6 controls.<sup>25</sup> To extend this finding, we performed RNA sequencing (RNA-seq) analyses on splenic Tfh cells gated as CD44<sup>+</sup>PSGL-1<sup>lo</sup>PD-1<sup>+</sup>CD4<sup>+</sup> (ref. 22) from anti-dsDNA immunoglobulin G (IgG)-positive TC and age-matched B6 mice (Figure S1), and the results were compared with microarray analyses. The juxtaposition of the transcriptional profiles obtained with different platforms and gating indicated a concerted perturbation of gene expression in TC Tfh cells (Figures 1A and 1B). Most significant differentially expressed genes (DEGs) shifted concordantly higher or lower in TC Tfh cells compared to B6 controls. This was especially true for genes related to Tfh development such as *Bcl6*, *Gata3*, and *Ii4*, which showed a higher expression in TC Tfh cells, and interferon regulatory factor 4 (*Irf4*) and Slam family 1 (*Slamf1*) that showed a higher expression in B6 Tfh cells (Figure 1A). 342 and 409 DEGs with fold changes (FCs) above 1.5 and false discovery rate (FDR)-corrected,  $p < 0.05$ , were respectively higher and lower in TC Tfh cells concordantly in both cohorts (Figure 1C). This DEG set represents a robust transcriptional signature of TC Tfh cells. When computed with publicly available gene sets, these shared DEGs matched with immune cell function and signaling, proliferation, and amino acid transport (Figure 1D), consistent with our previous findings.<sup>25</sup> DEGs higher in TC Tfh cells were enriched in multiple cellular signaling pathways (e.g., signaling by receptor Tyrosine kinase, tyrosine-protein kinase Met, and G protein-coupled receptors (GPCR)), suggesting that TC Tfh cells rely on higher signaling networks than B6 controls (Figure 1D). Additionally, gene set enrichment analyses (GSEAs) performed on these shared DEGs identified several metabolic pathways consistently enriched in either TC or B6 strains. Surprisingly, most of these pathways, including glycolysis/gluconeogenesis, the pentose phosphate pathway (PPP), OXPHOS, and the TCA cycle, were suppressed in TC Tfh cells compared to B6 controls (Figure 1E). On the other hand, two pathways directly involved in T cell activation, glycerophospholipid metabolism, and phosphatidylinositol signaling were elevated in TC Tfh cells (Figure 1E). To further test the robustness of

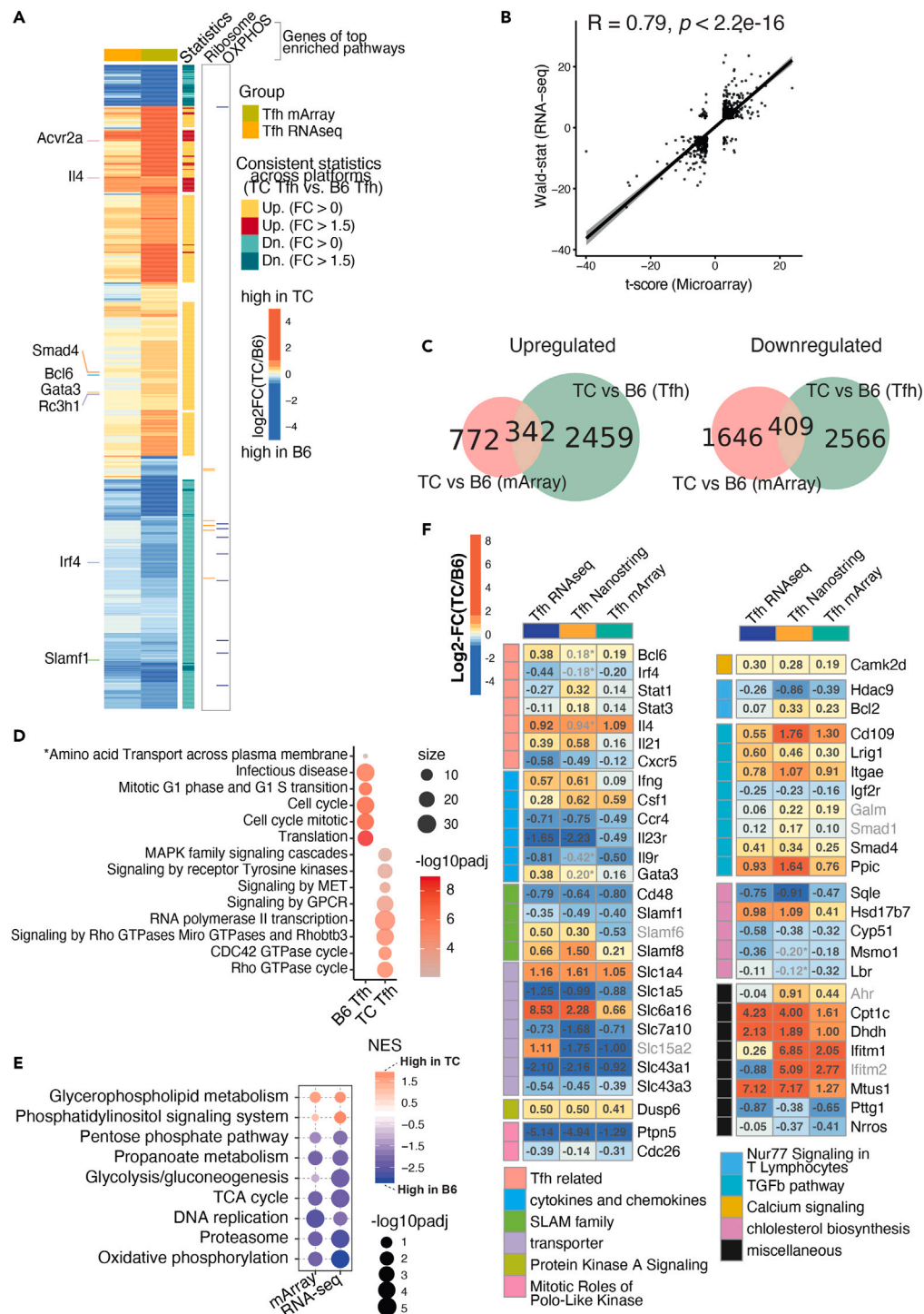


**Figure 1. Validated transcriptional programs in TC Tfh cells across platforms, gating strategies, and cohorts**

Combined analysis of the RNA-seq dataset (this report) from Tfh cells defined as CD44<sup>+</sup> PSGL-1<sup>lo</sup> PD-1<sup>+</sup>CD4<sup>+</sup> isolated from anti-dsDNA IgG-positive TC mice (n = 3) and B6 counterparts (n = 4) and Microarray (mArray) and Nanostring data from Tfh cells defined as PD1<sup>hi</sup> CXCR5<sup>+</sup> CD4<sup>+</sup> from TC (n = 5) and B6 (n = 3) mice (ref. <sup>25</sup>).

(A) Heatmap of log<sub>2</sub>FC comparing TC vs. B6 Tfh cells computed from the mArray and RNA-seq datasets. Selected genes related to Tfh function are shown on the left. DEGs with upregulation/downregulation consistent across platforms between TC and B6 are annotated on the right along with genes of interest belonging to two metabolic pathways,

**Figure 1. Continued**

OXPHOS, and ribosome, (B) Pearson correlation analysis of transcriptional profiles represented by t-scores from mArray (X axis) or Wald-statistic scores from RNA-seq (Y axis) datasets. (C) Venn diagrams visualizing shared DEGs upregulated (left) and downregulated (right) in TC relative to B6 Tfh cells between mArray (pink) and RNA-seq (green) datasets. DEGs were filtered with FDR-corrected  $p < 0.05$  in either direction. (D) Gene set overlap test of the canonical pathways representing the 342 DEGs upregulated in TC and 409 DEGs upregulated in B6 Tfh cells shown in C. The color scale indicates levels of significance, and the size of the symbols indicates the number of significant genes in each pathway. The gene sets are from the canonical pathway database. The asterisk ("Amino Acid Transport") indicates a pathway obtained from a separate analysis on DEGs filtered by FDR-corrected  $p < 0.05$  and fold change  $> 1.5$ . (E) Significant gene sets derived from GSEA analysis comparing TC and B6 Tfh cells in either RNA-seq or mArray, filtered by FDR-corrected  $p < 0.25$ . The color scale indicates normalized enrichment scores (NES), and the size of the symbols indicates levels of significance. (F) Heatmaps of DEGs between TC and B6 Tfh cells whose expression was concordant across three platforms, RNA-seq, mArray, and Nanostring, each in a different cohort of mice. The log<sub>2</sub>FC for each platform are shown in each cell, with the color indicating the size and direction of the change according to the scale shown in the upper left corner. DEGs were selected if they trended in the same direction between any of two assays (FDR-corrected  $p < 0.1$ ) with a few exceptions with  $p > 0.1$  labeled with asterisk (\*) and grayed out. The names of DEGs with direction consistent across only two platforms are also grayed out. DEGs were grouped by functions indicated to the left, with the corresponding keys at the bottom of the graph.

our transcriptional profiling, we incorporated a previously generated Nanostring dataset comparing TC and B6 Tfh cells.<sup>25</sup> Again, clearly consistent patterns were observed across the three platforms, highlighting an elevated expression of Tfh-related genes (e.g., *Bcl6*, *Il4*, and *Il21*), a dysregulated expression of SLAM family genes (e.g., *Slamf1*, *Cd48*) and solute transporters (e.g., *Slc1a4*, *Slc7a10*), and an increased expression of signaling molecules (e.g., *Dusp6*, *Camk2d*) in TC Tfh cells (Figure 1F). We have thus identified across three platforms and two gating strategies a robust transcriptional signature of TC Tfh cells that includes not only Tfh-related genes but also genes involved in immune activation as well as metabolism.

**TC Tfh cells express a canonical Tfh signature**

To shed light on whether TC Tfh cells undergo a distinct differentiation process from naive (Tn) CD4<sup>+</sup> T cells, we compared the transcriptional profile of CD44<sup>+</sup> Tn cells (Figure S1) to the corresponding Tfh cells from the same TC and B6 mice. Principal-component analyses (PCAs) revealed distinct transcriptional profiles among the 4 groups (Figure S2A). Cell-type differences across principal component (PC) 1 explained 82% of the variance and strain differences across PC2 accounted for only 12% of the variance. Therefore, these data demonstrated a greater difference between Tn and Tfh cells in both strains than between lupus-prone and control T cells from either subset. Of note, similar PC1 coordinates were shared between the clusters of Tfh cells isolated from TC or B6 mice, and likewise, similar PC2 coordinates were shared between their progenitor Tn cells. It suggests that although TC Tfh cells differ from B6 Tfh cells, the differential transcriptional projection from Tn to Tfh cells is largely shared between TC and B6 mice. This conclusion was supported by their Euclidian distance matrix (Figure S2B). Accordingly, the majority of significant DEGs either upregulated or downregulated between Tfh and Tn cells were shared between strains (Figure S2C). We then performed GSEA analyses and juxtaposed the significant gene sets computed on the ranked list of comparisons between Tfh and Tn cells from either TC or B6 mice. Expectedly from the PCA, gene sets differentially expressed between Tfh and Tn cells were largely shared between the TC and B6 strains. Gene sets related to T cell activation (e.g., cytokine activity/binding and signaling receptor binding) were increased in Tfh cells while gene sets involved in RNA binding decreased in Tfh cells (Figure S2D). A heatmap of Tfh-signature genes highlighted numerous genes (e.g., *Maf*, *Icos*) whose expression levels differed to a similar extent between Tfh and Tn cells in both TC and B6 strains (Figure S2E). However, some DEGs between Tn and Tfh cells showed a different expression between strains (Figure S2F). Some Tfh-upregulated DEGs were overexpressed in TC Tfh cells (e.g., *Bcl6*, *Il21*), and some in B6 Tfh cells (e.g., *Irf4*, *Batf*). A smaller group of genes were downregulated in Tfh cells and to a greater extent in TC (*Ifngr1*, *Itgb7*) or B6 (e.g., *Smad4*, *Prkd2*, and *Foxp1*) Tfh cells. These results suggest that the genetic susceptibility to lupus in TC mice exerts modulatory effects on the transcriptional profiles of Tfh cells. In conclusion, Tfh cells from lupus-prone mice express canonical Tfh-signature genes shared with non-autoimmune B6 mice. However, a subset of these genes presented a differential expression between the two strains.

**TC Tfh cells share a majority of DEGs relative to B6 Tfh cells with their Tn precursors**

To further identify the transcriptional perturbations exerted by the lupus-susceptibility genes on Tfh cells, we compared the transcriptional profiles from either Tfh or Tn cells isolated from TC mice with their

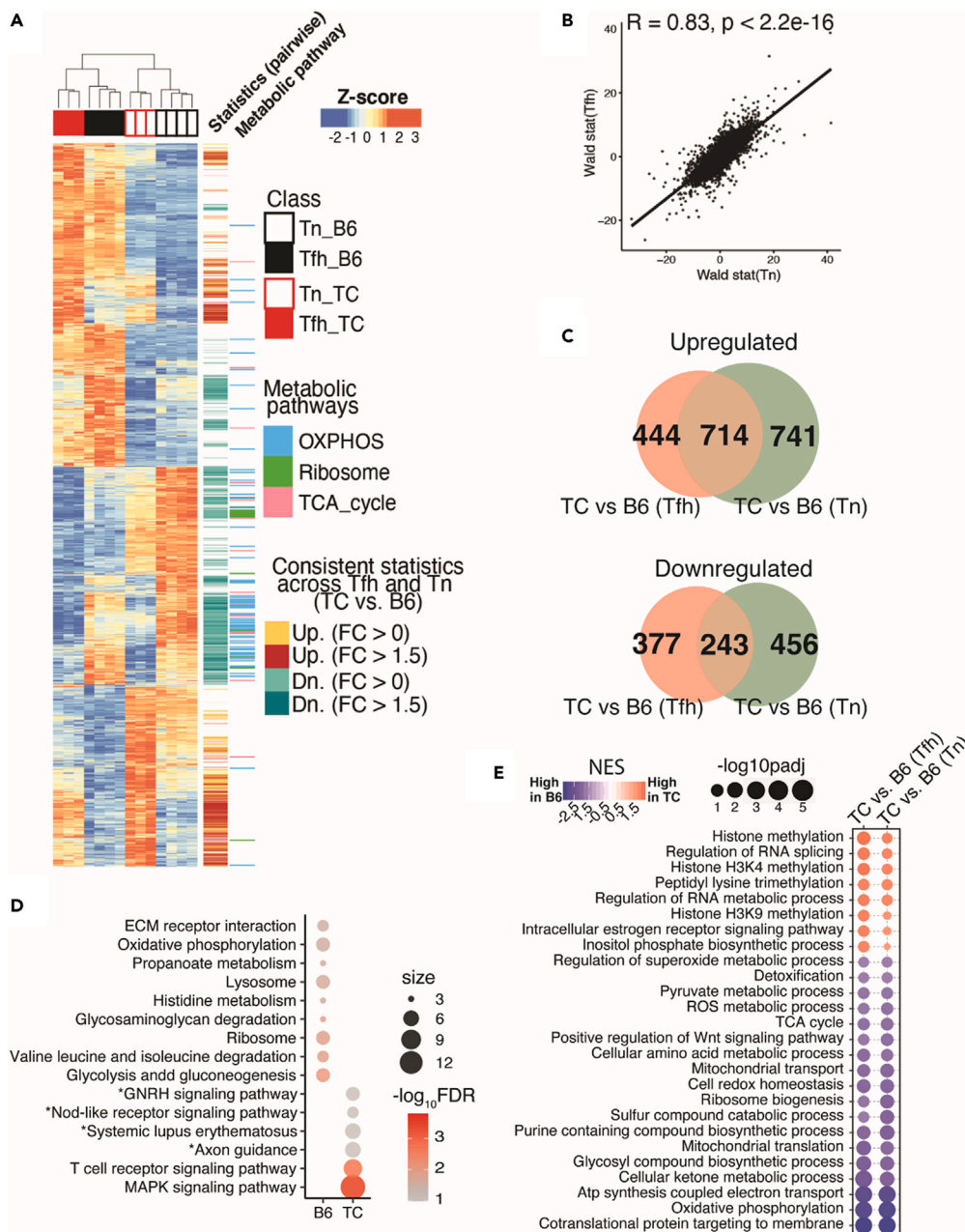


**Figure 2. Shared transcriptional signatures of TC Tn and Tfh cells relative to their B6 counterparts**

(A) Heatmap showing Z-scores transformed from regularized-Log2-converted counts of the whole transcriptional profile of DEGs (FDR-corrected  $p < 0.05$ , likelihood ratio test) in the 4 groups. The track on the right shows consistently upregulated DEGs comparing TC to B6 in both Tfh and Tn cells as labeled in yellow (FC > 0) or red (FC > 1.5); the consistently downregulated counterparts are labeled in cyan (FC > 0) or dark cyan (FC > 1.5). DEGs categorized in the indicated metabolic pathways are also highlighted in the further right track.

(B) Pearson correlation analyses of transcriptional profiles comparing Wald-statistic scores of the comparison of TC Tfh vs. B6 Tfh (Y axis) and the scores of the comparisons of TC Tn vs. B6 Tn (X axis).

(C) Venn diagrams visualizing DEGs (FDR-corrected  $p < 0.05$ , FC > 1.5) comparing B6 to TC mice shared by Tfh and Tn cells. The non-shared DEGs are uniquely (bottom) or up- (top) regulated in Tfh (pink) or Tn (green) cells.

(D) Gene set overlap test of DEGs upregulated in either TC or B6 and shared by both Tfh and Tn comparisons with the same cutoff as in panel C. The color scale indicates levels of significance, and the size of the symbols indicates the number

**Figure 2. Continued**

of significant genes in each pathway. Pathways are filtered by FDR <0.05, except for pathways with an asterisk (FDR <0.15). The pooled gene sets are from the KEGG database from the Molecular Signature Database (MSigDB v5.2). (E) Bubble plot of gene sets significantly different between TC vs. B6 mice in both Tfh and Tn cells, filtered by FDR-corrected  $p < 0.05$ . The inputs are ranked gene lists based on Wald-statistic scores comparing TC vs. B6 in either Tfh or Tn cells. The gene sets are from Gene Ontology database.

counterparts B6 controls and highlighted the significant DEGs concordantly upregulated or downregulated between the TC and B6 strains across Tfh and Tn cells. A substantial number of DEGs in TC Tfh cells trended similarly in TC Tn cells (Figure 2A). This was further supported by Pearson correlation analyses between the Wald-statistic rank lists of genes computed by comparing TC Tfh to B6 Tfh cells and the rank list of genes computed by comparing TC Tn to B6 Tn cells (Figure 2B). Within rigorously defined DEGs obtained from the TC to B6 comparisons across Tfh and Tn cells, 714 genes out of 1899 were co-upregulated by TC T cells (over  $\frac{1}{3}$  of DEGs in either comparison), while 243 genes (about a quarter of DEGs in either comparison) were co-downregulated by TC T cells when comparing to B6 T cells (Figure 2C). To understand the function of these genes, we computed the TC-upregulated or B6-upregulated overlapping genes with publicly available gene sets. Noticeably, T cell receptor (TCR) signaling and mitogen-activated protein kinase (MAPK) signaling pathways are upregulated in both TC Tfh and Tn cells, while metabolic processes such as OXPHOS and glycolysis were reduced in both TC Tfh and Tn cells (Figure 2D), suggesting that numerous signaling and metabolic perturbations found in TC Tfh cells (Figure S2D) occur early at the Tn state.

To corroborate this hypothesis, we performed GSEA analyses on Tfh or Tn cells comparing TC and B6 origins. The top six pathways enriched in both TC Tfh and Tn cells compared to B6 controls were related to histone methylation and RNA splicing regulation, suggesting that a specific epigenetic landscape plays a critical role in establishing the identity of TC Tfh cells and that it is established early at the Tn stage (Figure 2E). A strong chromatin modification signature was found in TC Tfh cells, including genes encoding for histone lysine methyl transferases (e.g., H3K36me) associated with open chromatin marks (Figure S3A). Among them, *Smyd2* was overexpressed in TC Tfh relative to B6 Tfh cells (Figures S3B and S3C) and corresponded to increased relative levels of H3K36m2 in TC Tfh cells (Figures S3D and S3E). The inositol phosphate synthesis pathway was also elevated in TC Tfh and Tn cells, suggesting a higher TCR to phosphoinositide 3-kinase (PI3K) signal. On the other hand, the majority of gene sets downregulated in both TC Tfh and Tn cells corresponded to metabolic pathways, including OXPHOS and redox homeostasis as well as several indicators of mitochondrial functions, suggesting that the perturbed metabolic mode in Tfh cells is inherited early in their precursor Tn cells (Figure 2E). Thus, our results suggest that perturbations in the metabolic modes and epigenetic landscape that characterize TC Tfh cells have been initiated at the Tn stage. In support of this hypothesis, *in vitro* polarization of Tn cells from pre-autoimmune TC mice resulted in a higher frequency of Tfh cells than from age-matched B6 mice (Figures S4A and S4B). This suggests that lupus-susceptibility genes confer TC CD4<sup>+</sup> T cells a higher intrinsic ability to become Tfh cells.

**The TC Tfh transcriptional program increases differentiation and effector functions**

In addition to the large number of DEGs in both TC Tfh and Tn cells as compared to B6 T cells, 444 out of 1,158 (38%) Tfh DEGs were uniquely upregulated in TC Tfh cells and 377 out of 620 (60%) Tfh DEGs were uniquely downregulated in TC Tfh cells (Figure 2C). To better understand the contribution of these genes to the TC Tfh cell expansion and phenotypes, we scrutinized the expression of specific genes based on their known association with T cell functions (Figure 3A). In addition, whenever possible with a reliable detection by flow cytometry, we compared the protein expression of these genes on an independent cohort of mice (Figure 3B). The expression of several transcription factors was altered in TC Tfh cells. Among them, the decreased expression of *Irf4*, identified as part of the TC Tfh signature (Figure 1), was not found in TC Tn cells, and it was confirmed at the protein level. We confirmed that anti-apoptotic BCL-2 protein levels were higher in TC Tfh than B6 Tfh cells<sup>25</sup> and showed here that it was specific to TC Tfh cells (Figures 3A and 3B).

Two quintessential Tfh-type cytokines, IL-21 and IL-4, along with interferon (IFN)  $\gamma$  and IL-10, two T cell cytokines associated with lupus,<sup>29</sup> were highly expressed in TC Tfh cells relative to B6, although not as much as in TC Tn cells relative to B6 (Figure 3A). A higher expression of IFN $\gamma$  protein was confirmed in both TC Tn and Tfh cells (Figure S4C). We also observed a heightened expression of the critical signaling adapter *Jak3*

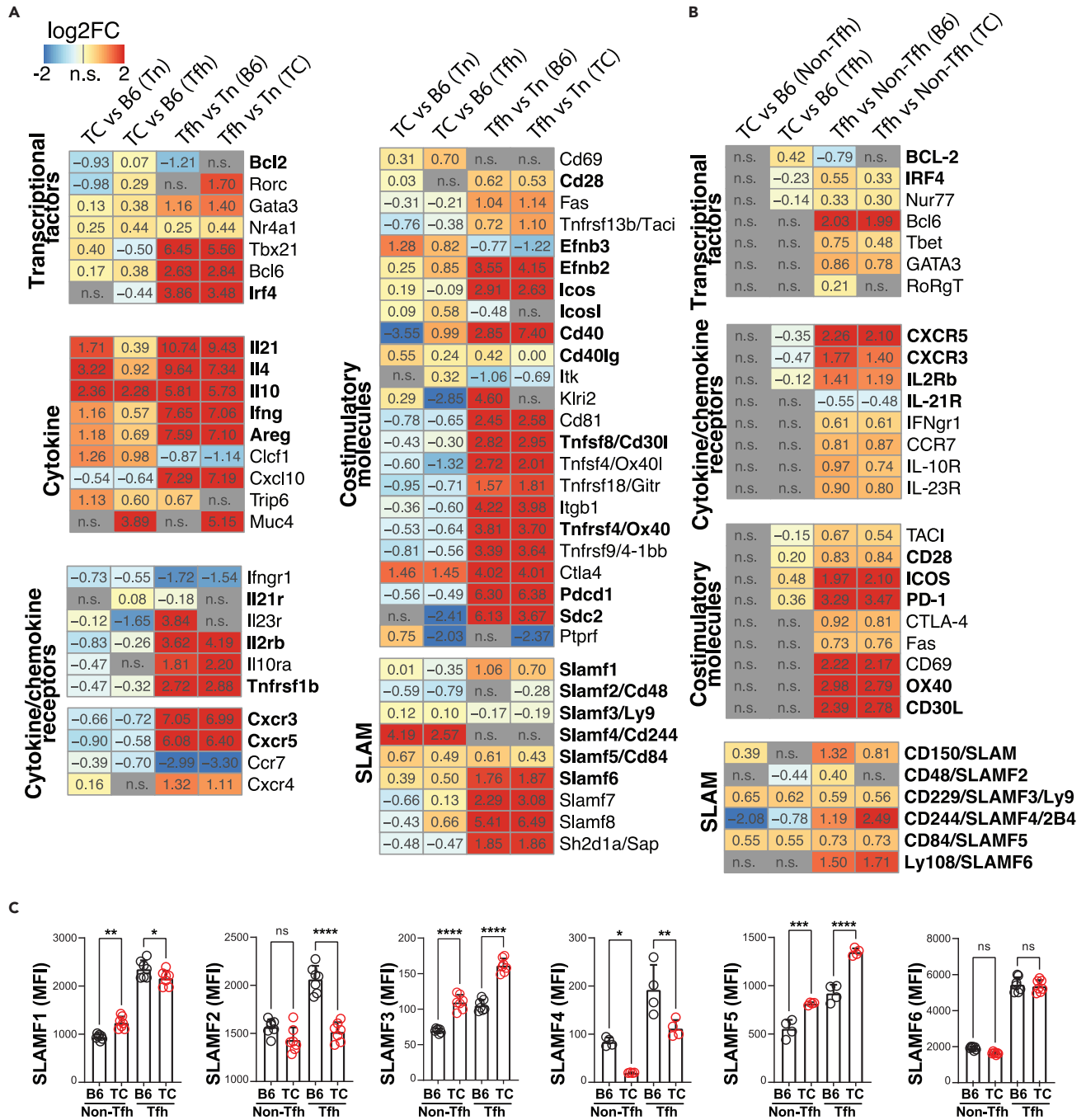


**Figure 3. Gene expression signature specific to Tfh cells of TC origin**

(A) Heatmaps for log<sub>2</sub>FC of significant DEGs (FDR-corrected p < 0.05) in each indicated comparison according to the color scale shown on the upper left. Genes were grouped by functional pathways indicated on the left of each cluster.

(B) Heatmaps for log<sub>2</sub>FC of protein levels of selected DEGs analyzed by flow cytometry. In (A) and (B), bold font indicates genes mentioned in the text.

(C) Flow cytometry analysis of SLAMF genes in non-Tfh and Tfh cells. Each symbol represents a mouse (n = 6–7) pooled from 2 experiments. Means ± s.e.m. analyzed by 1-way ANOVA with Dunnett's T3 multiple comparisons tests. \*p < 0.05, \*\*p < 0.01, \*\*\*p < 0.001.

acting downstream of both IL-21 and IL-4, as well as in genes in the Janus kinases - Signal transducer and activator of transcription (JAK-STAT) pathway (Figure S5A). The concerted increased expression of cytokines and signaling molecules downstream of their receptors may constitute an autocrine feedforward

loop amplifying Tfh cell development in TC mice. We also observed an elevated expression of non-canonical cytokine-like genes such as cardiotrophin-like cytokine (*Ccl1*), a member of the IL-6 family with B cell stimulating functions<sup>30</sup> and amphiregulin (*Areg*) that has been reported in Th2-type cells and in tissue-resident Treg cells,<sup>31</sup> potentially promoting pathogenic immune responses (Figure 3A). There was a small but significant increased expression of *Il21r* and a reduced expression of cytokine receptors specific to other lineages (*Il2rb* and *Tnfrsfb1*) in TC Tfh cells, although only IL-2R $\beta$  protein levels were also significantly reduced in TC Tfh cells (Figures 3A and 3B). Interestingly, a reduction in both mRNA and protein levels of Tfh-specific chemokine receptors including CXCR3 and CXCR5 was observed in TC Tfh cells, suggesting dysregulated cellular trafficking and migration (Figures 3A and 3B).

Other than cytokines, chemokines, and TCR signals, Tfh cells require co-stimulatory molecules to direct their development and sustain their activation. Although the levels of *Icos*, *Cd28*, and *Pdcd1* (encoding for PD1) were similar between TC and B6 Tfh cells, the corresponding protein levels were higher in TC Tfh cells (Figures 3A and 3B), implying post-translation layers of regulation in TC Tfh cells. Furthermore, the gene expression of another pivotal co-activating Tfh molecule, *Cd40lg* encoding for CD154, was increased in both TC Tn and Tfh cells (Figure 3A). In addition, upregulation of their ligands (*Cd40* and *Icosl*) was also observed on TC Tfh cells. The expression of other co-stimulatory molecules *Tnfrsf4* and *Tnfrsf8* was downregulated in TC Tfh cells, but it was not validated at the protein level for OX40 and CD30L. Elevated expression of *Efnb2/3*, which encodes for a nonclassical co-signaling molecule,<sup>32</sup> and the reduced expression of the TCR-recycling molecule *Sdc2*<sup>33</sup> were also observed, suggesting enhanced signaling rafts on the surface of TC Tfh cells.

Tfh cells are equipped with a broad array of SLAMF family members that regulate their contact with B cells.<sup>34</sup> Indeed, higher protein levels of SLAMF1 (CD150), SLAMF3 (Ly9), SLAMF4 (CD244), SLAMF5 (CD84), and SLAMF6 (Ly108) were found on Tfh cells compared to non-Tfh cells no matter their TC or B6 origin, and this was consistent with the RNA-seq data except for *Slamf3* (Figures 3A–3C). SLAMF5, one of the highest upregulated genes in TC Tfh cells (Figures 3A–3C), has been firmly established as positive regulator of interactions between murine Tfh and B cells,<sup>35</sup> and it is expressed by pathogenic human peripheral helper T (Tph) cells in rheumatoid arthritis.<sup>36</sup> SLAMF3 expression was also higher in TC Tfh and Tn cells in both RNA-seq and fluorescence-activated cell sorting (FACS) analyses, although whether it contributes to B cell help is unknown. On the other hand, the expression of SLAMF2 and SLAMF4 was lower in TC than B6 Tfh cells. Taken together, Tfh cells of TC origin manifest a perturbed expression of SLAMF genes, potentially altering their interactive dynamics with B cells.

TC Tfh cells presented an increased expression of type I and II (*Acvr2a* and *Acvr1b*) receptors for activin A (Figure S5A), a molecule that promotes human Tfh cell differentiation.<sup>37</sup> We also observed a higher expression of other genes in the activin receptor signaling pathway, such as transforming growth factor  $\beta$  (TGF $\beta$ ) signaling (*Tgfb3*, *Smad3*, and *Smad7*), suggesting that TC Tfh cells engage in heightened activin receptor signaling that intersects with TGF $\beta$  signaling. Activin A did not, however, enhance TC Tfh differentiation *in vitro* (data not shown). Therefore, the role of activin A in mouse Tfh cells in general and specifically in TC Tfh cells remains elusive.

Finally, TC Tfh cells presented a substantial number of DEGs in the highly overlapping mitogen-activated protein kinase (MAPK) and Kirsten rat sarcoma (K-Ras) pathways, which were also overexpressed, but to a lesser extent, in TC Tn cells (Figures S5A and S5B). This enhanced signaling may be secondary to a profound downregulation of the Phosphatase and tensin homolog (PTEN) pathway in both Tn and Tfh TC cells. These pathways are likely to play a major role in the enhanced differentiation, proliferation, and activation of TC Tfh cells. In conclusion, in-depth scrutinization of the Tfh-specific effector molecules and signaling pathways in TC mice at the transcriptional and protein levels revealed substantial alterations that not only may account for the accumulation of Tfh cells but also suggest that they develop enhanced effector functions.

### Both Tn and Tfh cells in TC mice express altered metabolic gene programs

We have previously reported a global increased mTOR expression in TC Tfh cells measured by histology as well as mTORC1 activity measured by flow cytometry on one of its targets, phospho-S6 (pS6) ribosomal protein.<sup>25</sup> Consistent with this finding, we found here an increased gene expression of the upstream p70-S6 kinase 1 *Rps6kb1* and the sensing amino acid transporters *Slc36a1* and *Slc38a9* (Figure S5A), both of which are critical for mTORC1 activation.<sup>38,39</sup> The protein expression of pS6 and p4EBP1, another marker of

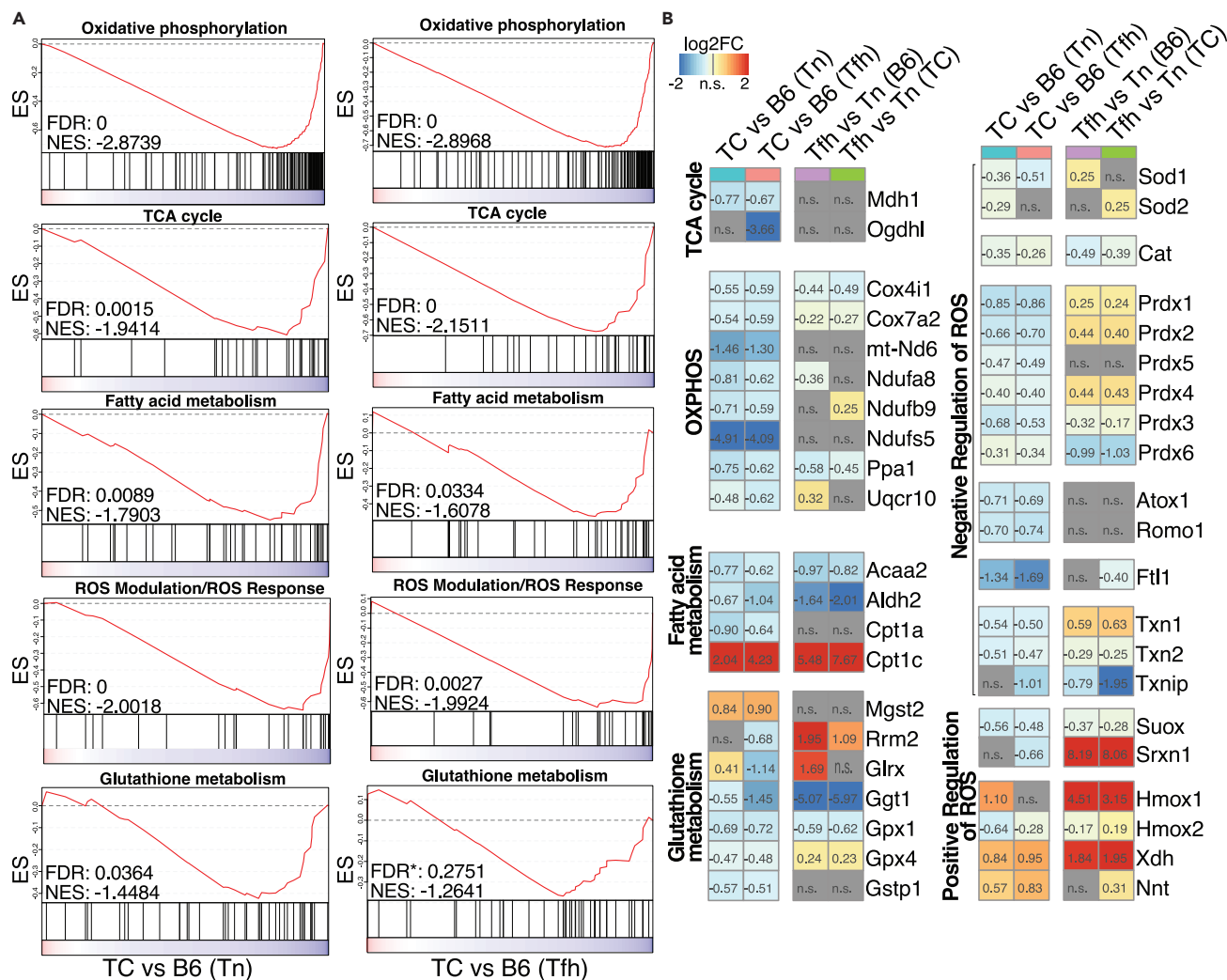


**Figure 4. Lupus-susceptibility genes confer mitochondrial defects in Tfh and Tn cells**

(A) GSEA plots on the indicated gene sets derived from the Molecular Signature Database. The inputs are ranked gene lists (Wald statistic) comparing separately TC and B6 Tfh cells on the left and Tn cells on the right. The asterisk associated with the FDR value for Glutathione metabolism indicates that this pathway did not meet the stringent significance threshold of FDR < 0.05. However, it was modestly significant with the FDR control and shared similar gene-rank profiles with TC Tn versus B6 Tn.

(B) Heatmaps of log<sub>2</sub>FC for DEGs (FDR-corrected p < 0.05) in the gene sets shown in (A).

mTORC1 activation, as well as protein kinase B phosphorylated at serine 473 (pAKT<sup>S473</sup>), a marker of mTORC2 activation, was elevated in Tfh cells relative to Tn cells (Figures S6A–S6C), confirming that Tfh cells rely on both mTORC1 and mTORC2 activation.<sup>23</sup> Concerning strain-wise differences, we found increased levels of pS6 not only in TC Tfh cells but also in TC Tn cells relative to their B6 counterparts (Figure S6B). Although the gene expression of the mTORC2 central regulator *Rictor* was elevated in TC Tfh cells relative to B6 (Figure S5A), pAKT<sup>S473</sup> expression was lower in TC than B6 Tfh cells (Figure S6C). This resulted in a skewed pS6/pAKT<sup>S473</sup> ratio between B6 and TC T cells (Figure S6D). Overall, these results show that TC CD4<sup>+</sup> T cells are sustained by an imbalanced mTORC1 activation that initiates in Tn cells and is maintained in Tfh cells.

Mitochondria directly tailor T cell effector functions,<sup>40,41</sup> and mitochondrial dysfunctions in T cells have been firmly associated with lupus.<sup>17,42,43</sup> However, mitochondria have not been specifically characterized in Tfh cells. The TC Tfh signature was characterized by decreased TCA cycle and OXPHOS pathways as compared to B6 Tfh cells (Figure 1E). A GSEA analysis also identified the downregulation of major mitochondrial pathways including OXPHOS, TCA cycle, and fatty acid (FA) metabolism in both Tfh and Tn cells from TC mice as compared to B6

counterparts (Figure 4A), suggesting that mitochondrial defects occurred early in TC Tn cells and were maintained when they differentiate into Tfh cells. Accordingly, genes essential for tricarboxylic acid (TCA) cycle (*Mdh1*, *Ogdh*) and OXPHOS (*Cox4i1*, *Ndufs5*, *Uqcrl0*) were downregulated in TC Tfh and Tn cells (Figure 4B). *Acaa2*, responsible for the last step of mitochondrial  $\beta$ -oxidation,<sup>44</sup> along with *Cpt1a* and *Alhd2*, was also downregulated (Figure 4B), indicating an impairment of FA oxidation in TC T cells. *Cpt1c* was upregulated in TC Tfh and Tn cells compared with B6 counterparts (Figure 4B). This atypical member of the carnitine palmitoyltransferase family functions as a lipid metabolism sensor and may favor triglyceride synthesis rather than FA oxidation.<sup>45</sup> We subsequently measured the uptake of BODIPY and 2-N-(7-nitrobenz-2-oxa-1,3-diazol-4-yl) amino-2-deoxyglucose (2-NBDG) to verify lipid and glucose metabolic activities *in vitro*. Tfh cells showed a higher lipid content as compared to Tn cells in both strains, but it was lower in both TC Tn and Tfh cells than in B6 counterparts (Figure S6E). Glucose uptake was also lower in TC T cells, both *in vitro* and *in vivo* (Figures S6F and S6G). It should be noted also that in the more physiological *in vivo* conditions, glucose uptake was globally lower in Tfh than in Tn cells (Figure S6G). These results suggest an altered nutrient flow in TC CD4<sup>+</sup> T cells including Tfh cells relative to B6 counterparts.

Mitochondrial dysfunction manifested not only in OXPHOS and FA metabolism but also in oxidative stress and redox imbalance exerted by uncontrolled production of reactive oxygen species (ROS), which plays a critical role in T cell activation in general<sup>46</sup> and in lupus in particular.<sup>47</sup> Indeed, gene sets associated with ROS modulation and glutathione metabolism were both dampened in TC Tfh and Tn cells compared to B6 T cells (Figure 4A). In agreement with the GSEA results, the expression of many genes related to glutathione metabolism, such as *Gpx1/4*, and negative regulation of ROS, such as *Sod1*, *Prdx1-6*, *Atox1*, and *Romo1*, was diminished in TC T cells (Figure 4B). *Gpx4* expression is required by Tfh cells to counterbalance high levels of lipid peroxidation and mitochondrial stress.<sup>48</sup> In contrast, we observed an increased expression of the gene encoding the mitochondrial (m) ROS-generating enzyme xanthine dehydrogenase (*Xdh*) (Figure 4B). Increase of nicotinamide nucleotide transhydrogenase (*Nnt*) (Figure 4B) may also promote a “reverse” electron flux from nicotinamide adenine dinucleotide phosphate (NADPH) to NADP<sup>+</sup>, consuming ROS-neutralizing NADPH.<sup>49</sup>

Globally, Tfh cells presented a reduced mitochondrial mass but an increased mitochondrial reactive oxygen species (mROS) and mitochondrial membrane potential (MMP) relative to Tn cells (Figures 5A–5D), indicating a mitochondrial involvement in this effector T cell subset. Importantly, differences were observed between B6 and TC T cells, with a lower mitochondrial mass in TC Tn and Tfh cells than in B6 counterparts and a higher mROS in TC Tfh than B6 Tfh cells. A reduced mitochondrial mass combined with an increased mROS validates the reduced expression of genes supporting mitochondrial metabolism as well as the dysregulation of genes related to antioxidant system TC Tfh cells. Due to limitations in Tfh cell numbers, we evaluated mitochondria by electron microscopy in CD44<sup>-</sup> Tn and CD44<sup>+</sup> effector T cells (Teff), which confirmed the reduction in mitochondrial size in B6 Teff relative to Tn cells, although their number was unchanged (Figures 5D–5F). The number of mitochondria increased in TC Teff cells, while their size remained similar between TC Tn and Teff cells, further supporting differential mitochondrial dynamics between B6 and TC CD4<sup>+</sup> T cells. Furthermore, Tn and specially TC Tfh cells expressed a robust gene signature that indicates a defective mitophagy, including the downregulation of *Pink1* and many genes involved in Pink/Parkin-mediated autophagy (Figures S7A–S7C). On the other hand, TC T cells overexpressed *Mterf3*, an inhibitor of mDNA replication,<sup>50</sup> which is required to maintain functional mitochondria. The overexpression of the mediator of fusion *Mfn1* in TC Tfh cells may be a response to an increased mitochondrial stress. In summary, our results indicate that the lupus-susceptibility genes that are expressed in TC mice trigger mitochondrial and antioxidant defects in Tn cells than are amplified in Tfh cells. This corresponds to the oxidative state that has been described in human SLE T cells<sup>51</sup> and suggests that it is a genetically controlled, intrinsic characteristic of lupus T cells that starts at the naive stage.

### TC Tfh cells present a distinctive anabolic metabolism

To further understand the metabolism of Tfh cells, we first reanalyzed the metabolomes of *in vitro*-polarized Tfh cells and activated T cells (Tact) from B6 mice.<sup>23</sup> Phosphatidylethanolamine (PE) and phosphatidylcholine (PC) synthesis pathways (Figure S8A), of which the end-products cytidine diphosphate (CDP)-ethanolamine and sn-Glycero-3-phosphocholine accumulated in Tfh cells while the substrates or intermediates, such as L-serine and choline, were significantly reduced (Figure S8B). Moreover, aspartate, an amino acid critical for T cell proliferation<sup>52,53</sup> was dramatically increased while other amino acids such as glycine and serine, fueling purine or PE synthesis,<sup>54</sup> were reduced (Figure S8B), consistent with a hyperactive

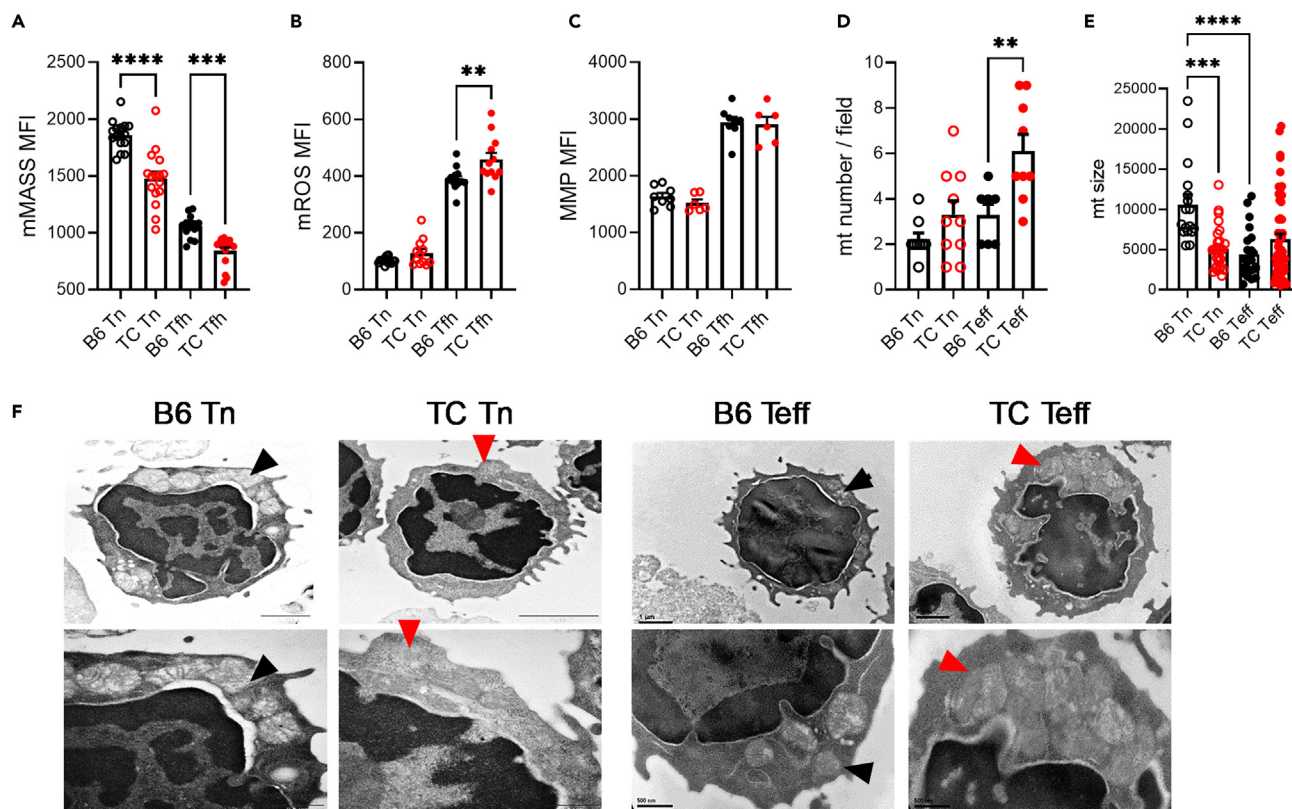


**Figure 5. Mitochondrial alterations in Tn and Tfh TC cells**

Mitochondrial mass (A), mROS (B), and (MMP (C), in Tn and Tfh cells from B6 and TC mice. Each symbol represents a mouse (n = 8–15 pooled from 2 to 4 cohorts).

(D–F) Number of mitochondria per cell (D) and mitochondria size (E) in Tn and Teff assessed by electron microscopy. Representative images are shown in (F) at  $\times 15,000$ – $20,000$  (top) and  $\times 40,000$  (bottom) magnification. Black and red arrow heads point to individual B6 and TC mitochondria, respectively. In (D), each point represents a cell (n = 7–10) from 5 mice per group, and (E) represents individual mitochondria from (F).

Means  $\pm$  SEM analyzed by 1-way ANOVA with Dunnett's T3 multiple comparisons tests. \*\*p < 0.01, \*\*\*p < 0.001, \*\*\*\*p < 0.0001.

malate-aspartate shuttle in Tfh cells driving aspartate synthesis (Figure S8A). Phosphatidylinositol phosphate (PIP) metabolism bridging TCR signaling with mTOR activation and anabolic processes was specifically heightened in Tfh cells. Accordingly, myo-inositol, the critical building block of this pathway, accumulated in Tfh cells (Figure S8B). Lactate levels were decreased in Tfh cells, indicating that glycolysis is not mobilized in B6 Tfh cells. However, TCA cycle intermediates, such as succinate, fumarate, and malate, were depleted while TCA byproducts itaconate and 2-hydroxyglutarate (2-HG) accumulated in Tfh cells, suggesting an active TCA cycle. Itaconate and 2-HG mitigate oxidative stress by inhibiting succinate dehydrogenase (*Sdh*) and  $\beta$ -ketoglutarate (KG)-mediated enzymatic reactions, respectively.<sup>55,56</sup> FA  $\beta$ -oxidation was downregulated in Tfh cells, as indicated by the reduced amounts of FA-conjugated carnitines. Tfh cells also presented increased levels of several metabolites related to pentose and glucuronate interconversions. Since the PPP generates NADPH to maintain the redox balance in activated T cells,<sup>57</sup> these data supports the need to mitigate stress responses in Tfh cells. Altogether, these observations indicate that Tfh cells are supported by mitochondrial metabolism and enhanced anabolic processes coupled with antioxidant responses to maintain redox balance.

To understand the metabolic processes that drive the hyperactive status of TC Tfh cells, we compared the metabolome of Tfh and Tn cells from TC and B6 mice. PCA of the 109 annotated metabolites demonstrated distinct profiles among the four groups (Figure 6A). We then performed pathway enrichment analyses comparing genotypes within the same cell types (TC vs. B6 Tfh and TC vs. B6 Tn) and comparing cell types within the same genotype (Tfh vs. Tn from TC mice and Tfh vs. Tn from B6 mice). A majority of significantly altered pathways, such as PC biosynthesis, purine metabolism, and aspartate metabolism, were shared

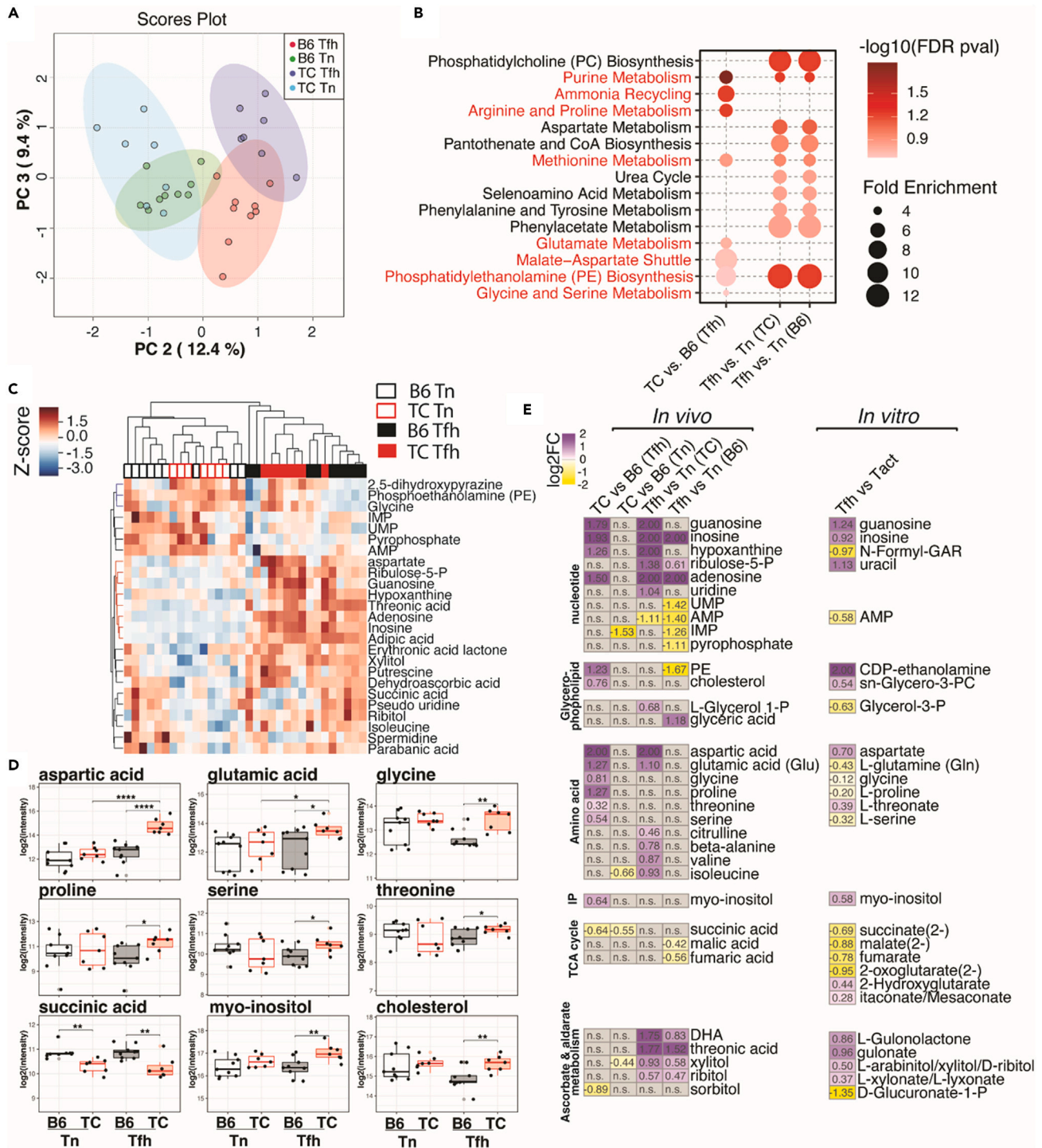


**Figure 6. Enhancement of anabolic metabolism in TC Tfh cells**

(A–D) GC-MS analysis was conducted on Tn and Tfh cells from TC or B6 mice from two cohorts. (A) Principal-component analysis (PC2 - PC3) of the 109 annotated metabolites. PC1 was ignored as it mainly accounted for batch effects,  $n = 7-9$ . (B) Pathway enrichment analysis of the significant metabolites (FDR-corrected  $p < 0.25$ , Student's  $t$  test) comparing TC vs. B6 Tfh, Tfh vs. Tn TC, and Tfh vs. Tn B6 cells. The TC vs. B6 Tn cell comparison did not show significant metabolite features. TC Tfh-specific pathways that are also significantly enriched in *in vitro*-activated Tfh cells are shown in red font (see Figure S8). (C) Hierarchical clustering analyses of significant metabolites with stringent criteria (FDR-corrected  $p < 0.05$ , one-way ANOVA) among the four indicated groups of T cells are shown by heatmap. (D) Selected metabolites differentially enriched in TC vs. B6 Tfh cells (nominal  $p < 0.05$ ) are shown by boxplots for the four groups of T cells. Means  $\pm$  SEM analyzed by 1-way ANOVA with Dunnett's T3 multiple comparisons tests. \* $p < 0.05$ , \*\* $p < 0.01$ , \*\*\*\* $p < 0.0001$ .

**Figure 6. Continued**

(E) Metabolic pathways shared between *ex vivo* Tfh cells compared to Tn cells shown in (A-D) and *in vitro*-polarized activated T cells (Tact) and Tfh cells.<sup>23</sup> The heatmaps show log<sub>2</sub>FC of selected significant metabolites, with the absolute numbers labeled in each cell and values with log<sub>2</sub>FC > 2 normalized to 2. DHA: dehydroascorbic acid; P: phosphate; PE: phosphatidylethanolamine; PC: Phosphatidylcholine; N-Formyl-GAR: 5'-Phosphoribosyl-N-formylglycinamide.

between TC and B6 mice when comparing cell types, suggesting that, as for the transcriptome, TC Tfh and B6 Tfh cells largely share metabolic programs (Figure 6B). However, several pathways were uniquely presented by TC Tfh cells compared to B6 Tfh cells, such as ammonia recycling, glutamate metabolism, and malate-aspartate shuttle, while PE biosynthesis and purine and methionine metabolism, which exist in B6 Tfh cells, were further enhanced in TC Tfh cells (Figure 6B). An increased PE synthesis and decreased degradation are an essential feature of Tfh cells to maintain CXCR5 surface expression.<sup>58</sup> A comparison of PE levels between Tn and Tfh cells confirmed this finding (Figure S9A). More interestingly, TC Tfh cells contained an increased amount of PE metabolite as well as an increased relative level of surface PE (Figure S9B). This process may compensate for a lower CXCR5 expression by TC Tfh cells (Figures 3A and 3B).

A hierarchical clustering analysis to visualize metabolites with levels that are rigorously altered among the four groups supported the pathway analysis by showing increased amounts of aspartate and several purine metabolites with Tfh cell differentiation, especially in TC Tfh cells (Figure 6C). This indicates enhanced anabolic activities in the Tfh cell development in TC mice. Further, PE and glycine levels were higher while succinic acid was less abundant in both Tn and Tfh cells isolated from TC mice when compared to B6 T cells (Figure 6C). As the same alterations in the levels of PE, glycine, and TCA intermediates were observed in *in vitro*-polarized B6 Tfh cells, this may indicate, as for gene expression, that metabolic programs in TC Tn cells favor Tfh cell development. We then compared the four groups with a lower threshold of significance (raw p value <0.05). This analysis confirmed the decreased levels of succinic acid in TC Tn and Tfh cells (Figure 6D). It also revealed that cholesterol, a critical component of lipid rafts in human lupus T cells,<sup>59</sup> was also more abundant in TC Tfh cells (Figure 6D). Together with the observation of an enhanced PE biosynthesis, this may reflect that TC Tfh cells require a robust lipid biosynthesis to facilitate the generation of immune synapses with GC B cells.<sup>60</sup> Finally, several amino acids other than glycine and aspartate were more abundant in TC Tfh cells (Figure 6D). Although glycine and serine that are used for anabolic metabolic processes<sup>54</sup> were depleted in B6 Tfh cells differentiated *in vitro*, their increase in *ex vivo* TC Tfh cells may reflect their enhanced capacity for amino acid intake. This corresponds to the enrichment in amino acid transporter pathway in TC Tfh cells observed in transcriptional analyses (Figure 1). Furthermore, we performed a network analysis of the dynamics of amino acid content and their transporters (AATs) in Tfh and Tn cells of TC or B6 origin by combining RNA-seq and metabolomic results (Figure S10). Expression of the majority of AATs was higher in Tfh than Tn cells (Figures S10A and S10B). Multiple AATs responsible for transporting glutamine (e.g., *Slc1a5*, *Slc38a6*, *Slc38a2*) were overexpressed in Tfh cells of both TC and B6 origins, but they were further enhanced in TC Tfh cells, consistent with the highest levels of glutamic acid detected in TC Tfh cells (Figures 6D and S10C). Moreover, the relative distribution of these glutamine transporters was different with *Slc1a5* dominating B6 Tfh and *Slc38a2* dominating TC Tfh cells. The activation of *Slc1a4* and *Slc36a1* in TC Tfh cells may explain the increased levels of serine and glycine comparing TC and B6 Tfh cells, respectively (Figure S10C).

Finally, the comparative analysis of the metabolites between the *in vitro* polarization results obtained in B6 Tfh cells<sup>23</sup> and the *ex vivo* results generated in this study confirmed several concerted alterations during Tfh cell development (Figure 6E). In addition, TC Tfh cells present further increases in nucleotide, glycerophospholipid, and amino acid metabolism, which are the hallmarks of anabolic processes optimal for T cell activation proliferation.<sup>52</sup> TCA cycle intermediates (e.g., succinate) were less abundant in TC Tfh cells, as they were in *in vitro*-polarized B6 Tfh cells, which aligned with the global downregulation of the expression of genes related to the TCA cycle (Figure 2) as well as mitochondrial alterations (Figure 4). Although metabolites relevant to ascorbate and aldarate metabolism were more abundant in both *in vivo* and *in vitro* Tfh cells comparing to their respective Tn cells, the levels of those metabolites were lower comparing TC Tfh/Tn to B6 Tfh/Tn cells. Given the TC Tfh cell phenotypes, such findings may confirm an unbalanced redox balance in TC Tfh cell leading to dysregulated T cell activation status.

**DISCUSSION**

The expansion of Tfh cells represents a common feature of most autoimmune diseases. A number of hypotheses have been proposed to explain this finding, including the fact that several genes associated

with susceptibility to autoimmune diseases also regulate the development of Tfh cells.<sup>61</sup> Tfh cells from TC mice are highly proliferative, resulting in an expansion of their number as the mice age.<sup>25</sup> Yet whether the lupus-susceptibility genes also favor effective and even pathogenic Tfh cell phenotypes was not fully investigated. We confirmed a robust transcriptional signature of TC Tfh cells, and we showed that this signature emerges first in TC Tn cells, providing strong evidence for a genetic basis. Histone modifications are likely to be involved in the TC Tn cells being poised to differentiate into Tfh cells since we observed a histone modification transcriptional signature in TC Tn cells that is expanded in Tfh cells.

TC Tfh cells share a canonical Tfh signature with control Tfh cells<sup>62</sup> by upregulating key Tfh-specific TFs (e.g., *Maf*, *Ascl2*, *Tox*, and *Tox2*) and surface markers (e.g., *Ccr6*, *Tigit*, and *Icos*). In addition, TC Tfh cells manifest a transcriptional state prone to increase differentiation and effector functions. The Tfh-specific cytokines IL-21 and IL-4 were drastically increased by the TC genetic background. TC Tfh cells also express *Ifng*, as well as Th2-specific *Gata3* and *Areg*, suggesting a Tfh2-type phenotype, which correlates with disease severity in SLE patients.<sup>63</sup> Therefore, TC Tfh cells are characterized by the enhancement of multiple cytokines that empower their effector and pathogenic function. These cytokines may participate into a feedforward loop by enhanced downstream JAK-STAT and MAPK signaling and may result from an increased KRAS signaling that also promotes cell proliferation. TC Tfh cells also showed a reduced expression of IRF4, which integrates the strength of TCR signaling. IRF4 highest expression promotes T helper over Tfh cell differentiation.<sup>64</sup> Its decreased expression in TC Tfh cells suggests a lower tonic TCR signaling attributed to chronic activation by autoantigens, which might enhance Tfh differentiation.<sup>65</sup> Tfh cells help GC B cells through an immunological synapse, where they interact with each other through membrane-bound signals including from the SLAMF family (SLAMF) receptors. The requirement for the expression of SLAMF genes for Tfh cell differentiation is controversial, in part due to their overlapping roles and function as both receptors and ligands.<sup>66</sup> We showed here that each of the 6 SLAMF genes is upregulated in Tfh cells at both transcriptional and translational levels. Furthermore, TC Tfh cells expressed higher levels of SLAMF3 and SLAMF5 but lower levels of SLAMF2 and SLAMF4 than B6 Tfh cells. SLAMF molecules induce either positive or negative signals in a context-dependent manner. The integration of these signals from several SLAMF members on both Tfh and B cells determines the functional outcomes.<sup>67</sup> The significance of the differential expression of SLAMF members on TC Tfh cells will require functional assays with B cells from either TC or B6 mice.

The transcriptomic analysis showed extensive alterations in metabolic pathways that started in in TC Tn cells and were amplified in Tfh cells. Our initial reporting of increased mTORC1 activation in TC Tfh cells<sup>25</sup> was confirmed and extended to mTORC2. mTORC1 and mTORC2 contribute to specific aspects of Tfh cell differentiation and functions,<sup>23</sup> and their enhanced activation in lupus may support the same functions. mTORC2 deficiency reduced the frequency of Tfh cells along with other alterations in T cell phenotypes in a mouse model of autoimmunity.<sup>68</sup> The enhanced mTOR activation in TC Tfh cells is therefore not unique to this subset and corresponds to the high mTOR activity that characterizes lupus T and B cells.<sup>69</sup>

Besides mTOR activation, mitochondrial pathways were the most affected in both TC Tn and Tfh cells. Mitochondrial defects have been reported in the T cells of SLE patients with increased mitochondrial mass and MMP.<sup>70</sup> TC Tfh cells have a decreased mitochondrial mass, unchanged MMP, and increased mROS, which mirrors the phenotype of *Sle1c2* CD4<sup>+</sup> T cells with reduced *Esrrg* expression or *Esrrg*-deficient T cells.<sup>71,72</sup> It is therefore likely that the low *Esrrg* expression in TC T cells plays a major role in their dysfunctional mitochondria. In addition, TC Tfh cells presented an altered mitophagy gene signature. A dysfunctional mitophagy has been proposed as a major contributor to T cell defects in SLE patients, via mechanisms including the unrestrained production of mROS.<sup>43,70,73,74</sup> Impaired mitophagy has also been linked to autoimmunity through the generation of interferogenic mtDNA.<sup>75</sup> Furthermore, TC T cells overexpressed *Mterf3*, a gene that inhibits the initiation of mtDNA transcription. Mitochondrial fitness directly depends on mtDNA replication and transcription, which when impaired, forces the cells to rely on glycolysis.<sup>76</sup> Accordingly, TC T cells showed a profound downregulation of the OXPHOS, TCA cycle, and FA oxidation pathways, along with an upregulation of oxidative stress pathways. Thus, TC mitochondria are likely to be poor energy producers, which could be the root cause of the TC Tfh cells being highly sensitive to the inhibition of glucose metabolism.<sup>25</sup>

The transcriptional alterations in TC Tfh cells culminated with metabolic changes that correlated with differential expression profiles of solute transporters, especially for amino acid transport. There is increasing

evidence that amino acid metabolism represents a critical checkpoint in T cell activation.<sup>77</sup> Glutamine metabolism has been so far the only amino acid investigated in lupus, including in TC Tfh cells,<sup>25</sup> and results obtained here suggest that glutamine import play a central role in TC Tfh cells. Specific anabolic pathways such as ammonia recycling, glutamate metabolism, and malate-aspartate shuttle dominated the metabolic profile of TC Tfh cells. The malate-aspartate shuttle provides aspartate to helper T cells that is required for their proliferation.<sup>52</sup> Ammonia recycling is a process by which nitrogen is repurposed for amino acid synthesis, including aspartate, in highly proliferating cells.<sup>78</sup> These two processes are likely to support TC Tfh cell proliferation and expansion. The increased glutamate metabolism corresponded to a greater glutamine import. It is unlikely to correspond to an increased mitochondrial glutamine metabolism due to the low expression of TCA genes but most likely to support the chromatin modification signature found in TC Tfh cells, as it has been shown for Th1 cells.<sup>27</sup>

Overall, the transcriptomic and metabolic analyses of TC Tfh cells suggest that lupus Tfh cells expand from naive T cells that are poised to differentiate into the follicular helper pathway, potentially through epigenetic modifications sustained by glutamine metabolism. TC Tfh cells combine the canonical Tfh signature with a gene expression program that increases their effector functions. TC Tfh cells also undergo a profound metabolic reprogramming that impairs mitochondrial functions and redirects amino acid metabolism toward the greater demands of highly proliferating cells. These alterations may offer targets for an elimination of T cell help that licenses pathogenic autoantibodies.

### Limitations of the study

This study was limited to one lupus-prone mouse model, and human data were not included. Further, mechanistic experiments following up the results presented were not performed. This study was designed to investigate classical Tfh cells, although we used two different gating strategies, one of them using CXCR5, to define the TC Tfh signature. The frequency of CXCR5<sup>-</sup> CXCR3<sup>+</sup> PD-1<sup>hi</sup> Tph cells is also expanded in SLE patients with a high capacity to provide B cell help.<sup>79–81</sup> On the other hand, the frequency of CXCR3<sup>+</sup> Tfh1 is decreased in SLE patients,<sup>82</sup> and the frequency of circulating CXCR3<sup>-</sup>PD-1<sup>+</sup>CD4<sup>+</sup>T cells correlates with disease activity.<sup>83</sup> Our findings of decreased CXCR3 and CXCR5 may reflect an expansion of these corresponding populations in the TC lupus-mouse model in which an increased frequency of extrafollicular helper T cells has also been reported.<sup>84</sup> The current metabolomics study is based on a relatively small number of identified metabolites with a preference for volatile organic compounds inherited by the limitations of gas chromatography-mass spectrometry (GC-MS) analytical platform. Encouraged by the significance of presented metabolic signatures, deeper and targeted approaches (e.g., liquid-chromatography-MS-based methods) would be of great promise.

### STAR★METHODS

Detailed methods are provided in the online version of this paper and include the following:

- KEY RESOURCES TABLE
- RESOURCE AVAILABILITY
  - Lead contact
  - Data and code availability
- EXPERIMENTAL MODEL AND SUBJECT DETAILS
- METHOD DETAILS
  - Flow cytometry and cell sorting
  - RNA sequencing
  - Western blot and qRT-PCR analysis
  - *In vitro* Tfh cells polarization
  - Electron microscopy
  - Metabolomic analyses
- QUANTIFICATION AND STATISTICAL ANALYSIS

### SUPPLEMENTAL INFORMATION

Supplemental information can be found online at <https://doi.org/10.1016/j.isci.2023.106774>.

## ACKNOWLEDGMENTS

This study was supported by grants from the NIH R01 AI154630 to M.M. and L.M. and R01 DK105550 to JCR. We are grateful to Dr. Hongbo Chi for allowing access to some of his published data and to members of the Morel lab for discussions. We acknowledge the excellent services from the UF ICBR sequencing and electron microscopy cores, as well as from the UC Davis West Coast Metabolomics Center.

## AUTHOR CONTRIBUTIONS

Conceptualization, M.G., S.C.C., M.M., and L.M.; Methodology, M.G. and S.C.C.; Investigation, M.G., S.C.C., Y.P.P., X.Z., A.S.E., and V.A.G.; Writing – Original Draft, M.G. and L.M.; Writing – Review & Editing, M.G., S.C.C., and L.M.; Funding Acquisition, L.M.; Resources, J.C.R.; Supervision, J.C.R., M.M., and L.M.

## DECLARATION OF INTERESTS

Dr. Jeffrey Rathmell is a founder, scientific advisory board member, and stockholder of Sitryx Therapeutics, a scientific advisory board member and stockholder of Caribou Biosciences, a member of the scientific advisory board of Nirogy Therapeutics, has consulted for Merck, Pfizer, and Mitobridge within the past three years, and has received research support from Incyte Corp., Calithera Biosciences, and Tempest Therapeutics. The other authors declare no competing interests.

## INCLUSION AND DIVERSITY

One or more of the authors of this paper self-identifies as a gender minority in their field of research. While citing references scientifically relevant for this work, we also actively worked to promote gender balance in our reference list.

Received: January 17, 2023

Revised: March 28, 2023

Accepted: April 24, 2023

Published: April 26, 2023

## REFERENCES

- Craft, J.E. (2012). Follicular helper T cells in immunity and systemic autoimmunity. *Nat. Rev. Rheumatol.* 8, 337–347. <https://doi.org/10.1038/nrrheum.2012.58>.
- Kim, S.J., Lee, K., and Diamond, B. (2018). Follicular helper T cells in systemic lupus erythematosus. *Front. Immunol.* 9, 1793. <https://doi.org/10.3389/fimmu.2018.01793>.
- Mountz, J.D., Hsu, H.C., and Ballesteros-Tato, A. (2019). Dysregulation of T follicular helper cells in lupus. *J. Immunol.* 202, 1649–1658. <https://doi.org/10.4049/jimmunol.1801150>.
- Sasaki, T., Bracero, S., Keegan, J., Chen, L., Cao, Y., Stevens, E., Qu, Y., Wang, G., Nguyen, J., Sparks, J.A., et al. (2022). Longitudinal immune cell profiling in patients with early systemic lupus erythematosus. *Arthritis Rheumatol.* 74, 1808–1821. <https://doi.org/10.1002/art.42248>.
- Bubier, J.A., Sproule, T.J., Foreman, O., Spolski, R., Shaffer, D.J., Morse, H.C., 3rd, Roopenian, D.C., Leonard, W.J., and Roopenian, D.C. (2009). A critical role for IL-21 receptor signaling in the pathogenesis of systemic lupus erythematosus in BXSB-Yaa mice. *Proc. Natl. Acad. Sci. USA* 106, 1518–1523. <https://doi.org/10.1073/pnas.0807309106>.
- Choi, J.Y., Seth, A., Kashgarian, M., Terrillon, S., Fung, E., Huang, L., Wang, L.C., and Craft, J. (2017). Disruption of pathogenic cellular networks by IL-21 blockade leads to disease amelioration in murine lupus. *J. Immunol.* 198, 2578–2588. <https://doi.org/10.4049/jimmunol.1601687>.
- Crotty, S. (2019). T follicular helper cell biology: a decade of discovery and diseases. *Immunity* 50, 1132–1148. <https://doi.org/10.1016/j.immuni.2019.04.011>.
- Vinuesa, C.G., Linterman, M.A., Yu, D., and MacLennan, I.C.M. (2016). Follicular helper T cells. *Annu. Rev. Immunol.* 34, 335–368. <https://doi.org/10.1146/annurev-immunol-041015-055605>.
- Morel, L., Croker, B.P., Blenman, K.R., Mohan, C., Huang, G., Gilkeson, G., and Wakeland, E.K. (2000). Genetic reconstitution of systemic lupus erythematosus immunopathology with polycongenic murine strains. *Proc. Natl. Acad. Sci. USA* 97, 6670–6675.
- Choi, S.C., Hutchinson, T.E., Titov, A.A., Seay, H.R., Li, S., Brusko, T.M., Croker, B.P., Salek-Ardakani, S., and Morel, L. (2016). The lupus susceptibility gene Pbx1 regulates the balance between follicular helper T cell and regulatory T cell differentiation. *J. Immunol.* 197, 458–469. <https://doi.org/10.4049/jimmunol.1502283>.
- Wandstrat, A.E., Nguyen, C., Limaye, N., Chan, A.Y., Subramanian, S., Tian, X.H., Yim, Y.S., Pertsemlidis, A., Garner, H.R., Morel, L., and Wakeland, E.K. (2004). Association of extensive polymorphisms in the SLAM/CD2 gene cluster with murine lupus. *Immunity* 21, 769–780.
- Chen, S., Cai, C., Li, Z., Liu, G., Wang, Y., Blonska, M., Li, D., Du, J., Lin, X., Yang, M., and Dong, Z. (2017). Dissection of SAP-dependent and SAP-independent SLAM family signaling in NKT cell development and humoral immunity. *J. Exp. Med.* 214, 475–489. <https://doi.org/10.1084/jem.20161312>.
- Ise, W., Fujii, K., Shiroguchi, K., Ito, A., Kometani, K., Takeda, K., Kawakami, E., Yamashita, K., Suzuki, K., Okada, T., and Kurosaki, T. (2018). T follicular helper cell-germinal center B cell interaction strength regulates entry into plasma cell or recycling germinal center cell fate. *Immunity* 48, 702–715.e4. <https://doi.org/10.1016/j.immuni.2018.03.027>.
- Keszei, M., Detre, C., Rietdijk, S.T., Muñoz, P., Romero, X., Berger, S.B., Calpe, S., Liao, G., Castro, W., Julien, A., et al. (2011). A novel isoform of the Ly108 gene ameliorates murine lupus. *J. Exp. Med.* 208, 811–822.
- Keszei, M., Detre, C., Castro, W., Magelky, E., O’Keeffe, M., Kis-Toth, K., Tsokos, G.C., Wang, N., and Terhorst, C. (2013). Expansion of an osteopontin-expressing T follicular helper cell subset correlates with autoimmunity in B6.Sle1b mice and is suppressed by the H1-isoform of the Slamf6

- receptor. *Faseb. J.* 27, 3123–3131. <https://doi.org/10.1096/fj.12-226951>.
16. Piranavan, P., Bhamra, M., and Perl, A. (2020). Metabolic targets for treatment of autoimmune diseases. *Immunometabolism* 2, e200012. <https://doi.org/10.20900/immunometab20200012>.
  17. Teng, X., Cornaby, C., Li, W., and Morel, L. (2019). Metabolic regulation of pathogenic autoimmunity: therapeutic targeting. *Curr. Opin. Immunol.* 61, 10–16. <https://doi.org/10.1016/j.coi.2019.07.001>.
  18. Teng, X., Brown, J., Choi, S.C., Li, W., and Morel, L. (2020). Metabolic determinants of lupus pathogenesis. *Immunol. Rev.* 295, 167–186. <https://doi.org/10.1111/imr.12847>.
  19. Yin, Y., Choi, S.C., Xu, Z., Perry, D.J., Seay, H., Croker, B.P., Sobel, E.S., Brusko, T.M., and Morel, L. (2015). Normalization of CD4+ T cell metabolism reverses lupus. *Sci. Transl. Med.* 7, 274ra18. <https://doi.org/10.1126/scitranslmed.aaa0835>.
  20. Choi, S.C., and Morel, L. (2020). Immune metabolism regulation of the germinal center response. *Exp. Mol. Med.* 52, 348–355. <https://doi.org/10.1038/s12276-020-0392-2>.
  21. Oestreich, K.J., Read, K.A., Gilbertson, S.E., Hough, K.P., McDonald, P.W., Krishnamoorthy, V., and Weinmann, A.S. (2014). Bcl-6 directly represses the gene program of the glycolysis pathway. *Nat. Immunol.* 15, 957–964. <https://doi.org/10.1038/ni.2985>.
  22. Ray, J.P., Staron, M.M., Shyer, J.A., Ho, P.C., Marshall, H.D., Gray, S.M., Laidlaw, B.J., Araki, K., Ahmed, R., Kaech, S.M., and Craft, J. (2015). The interleukin-2-mTORC1 kinase axis defines the signaling, differentiation, and metabolism of T helper 1 and follicular B helper T cells. *Immunity* 43, 690–702. <https://doi.org/10.1016/j.immuni.2015.08.017>.
  23. Zeng, H., Cohen, S., Guy, C., Shrestha, S., Neale, G., Brown, S.A., Cloer, C., Kishton, R.J., Gao, X., Youngblood, B., et al. (2016). mTORC1 and mTORC2 kinase signaling and glucose metabolism drive follicular helper T cell differentiation. *Immunity* 45, 540–554. <https://doi.org/10.1016/j.immuni.2016.08.017>.
  24. Merckenschlager, J., Finkin, S., Ramos, V., Kraft, J., Cipolla, M., Nowosad, C.R., Hartweger, H., Zhang, W., Olinares, P.D.B., Gazumyan, A., et al. (2021). Dynamic regulation of TFH selection during the germinal centre reaction. *Nature* 591, 458–463. <https://doi.org/10.1038/s41586-021-03187-x>.
  25. Choi, S.C., Titov, A.A., Abboud, G., Seay, H.R., Brusko, T.M., Roopenian, D.C., Salek-Ardakani, S., and Morel, L. (2018). Inhibition of glucose metabolism selectively targets autoreactive follicular helper T cells. *Nat. Commun.* 9, 4369. <https://doi.org/10.1038/s41467-018-06686-0>.
  26. Kono, M., Yoshida, N., Maeda, K., Suárez-Fueyo, A., Kyttaris, V.C., and Tsokos, G.C. (2019). Glutaminase 1 inhibition reduces glycolysis and ameliorates lupus-like disease in MRL/lpr mice and experimental autoimmune encephalomyelitis. *Arthritis Rheumatol.* 71, 1869–1878. <https://doi.org/10.1002/art.41019>.
  27. Johnson, M.O., Wolf, M.M., Madden, M.Z., Andrejeva, G., Sugiura, A., Contreras, D.C., Maseda, D., Libert, M.V., Paz, K., Kishton, R.J., et al. (2018). Distinct regulation of Th17 and Th1 cell differentiation by glutaminase-dependent metabolism. *Cell* 175, 1780–1795.e19. <https://doi.org/10.1016/j.cell.2018.10.001>.
  28. Dong, X., Antao, O.Q., Song, W., Sanchez, G.M., Zembruski, K., Koumpouras, F., Lemenze, A., Craft, J., and Weinstein, J.S. (2021). Type I interferon-activated STAT4 regulation of follicular helper T cell-dependent cytokine and immunoglobulin production in lupus. *Arthritis Rheumatol.* 73, 478–489. <https://doi.org/10.1002/art.41532>.
  29. Theofilopoulos, A.N., Dummer, W., and Kono, D.H. (2001). T cell homeostasis and systemic autoimmunity. *J. Clin. Invest.* 108, 335–340. <https://doi.org/10.1172/JCI12173>.
  30. Savin, V.J., Sharma, M., Zhou, J., Gennochi, D., Fields, T., Sharma, R., McCarthy, E.T., Srivastava, T., Domen, J., Tormo, A., and Gauchat, J.F. (2015). Renal and hematological effects of CLCF-1, a B-cell-stimulating cytokine of the IL-6 family. *J. Immunol. Res.* 2015, 714964. <https://doi.org/10.1155/2015/714964>.
  31. Zaiss, D.M.W., van Loosdregt, J., Gorlani, A., Bekker, C.P.J., Gröne, A., Sibilia, M., van Bergen en Henegouwen, P.M.P., Roovers, R.C., Coffey, P.J., and Sijts, A.J.A.M. (2013). Amphiregulin enhances regulatory T cell-suppressive function via the epidermal growth factor receptor. *Immunity* 38, 275–284. <https://doi.org/10.1016/j.immuni.2012.09.023>.
  32. Darling, T.K., and Lamb, T.J. (2019). Emerging roles for Eph receptors and ephrin ligands in immunity. *Front. Immunol.* 10, 1473. <https://doi.org/10.3389/fimmu.2019.01473>.
  33. Rovira-Clavé, X., Angulo-Ibáñez, M., Noguero, O., Espel, E., and Reina, M. (2012). Syndecan-2 can promote clearance of T-cell receptor/CD3 from the cell surface. *Immunology* 137, 214–225. <https://doi.org/10.1111/j.1365-2567.2012.03626.x>.
  34. Qin, L., Waseem, T.C., Sahoo, A., Bieerkehazhi, S., Zhou, H., Galkina, E.V., and Nurieva, R. (2018). Insights into the molecular mechanisms of T follicular helper-mediated immunity and pathology. *Front. Immunol.* 9, 1884. <https://doi.org/10.3389/fimmu.2018.01884>.
  35. Cannons, J.L., Qi, H., Lu, K.T., Dutta, M., Gomez-Rodriguez, J., Cheng, J., Wakeland, E.K., Germain, R.N., and Schwartzberg, P.L. (2010). Optimal germinal center responses require a multistage T cell:B cell adhesion process involving integrins, SLAM-associated protein, and CD84. *Immunity* 32, 253–265. <https://doi.org/10.1016/j.immuni.2010.01.010>.
  36. Rao, D.A., Gurish, M.F., Marshall, J.L., Slowikowski, K., Fonseca, C.Y., Liu, Y., Donlin, L.T., Henderson, L.A., Wei, K., Mizoguchi, F., et al. (2017). Pathologically expanded peripheral T helper cell subset drives B cells in rheumatoid arthritis. *Nature* 542, 110–114. <https://doi.org/10.1038/nature20810>.
  37. Locci, M., Wu, J.E., Arumemi, F., Mikulski, Z., Dahlberg, C., Miller, A.T., and Crotty, S. (2016). Activin A programs the differentiation of human TFH cells. *Nat. Immunol.* 17, 976–984. <https://doi.org/10.1038/ni.3494>.
  38. Kono, M., Maeda, K., Stocton-Gavanesu, I., Pan, W., Umeda, M., Katsuyama, E., Burbano, C., Orite, S.Y.K., Vukelic, M., Tsokos, M.G., et al. (2019). Pyruvate kinase M2 is requisite for Th1 and Th17 differentiation. *JCI Insight* 4, e127395. <https://doi.org/10.1172/jci.insight.127395>.
  39. Rebsamen, M., Pochini, L., Stasyk, T., de Araújo, M.E.G., Galluccio, M., Kandasamy, R.K., Snijder, B., Fauster, A., Rudashevskaya, E.L., Bruckner, M., et al. (2015). SLC38A9 is a component of the lysosomal amino acid sensing machinery that controls mTORC1. *Nature* 519, 477–481. <https://doi.org/10.1038/nature14107>.
  40. Baixauli, F., Acín-Pérez, R., Villarroya-Beltrí, C., Mazzeo, C., Nuñez-Andrade, N., Gabandé-Rodríguez, E., Ledesma, M.D., Blázquez, A., Martín, M.A., Falcón-Pérez, J.M., et al. (2015). Mitochondrial respiration controls lysosomal function during inflammatory t cell responses. *Cell Metabol.* 22, 485–498. <https://doi.org/10.1016/j.cmet.2015.07.020>.
  41. Liu, P.S., and Ho, P.C. (2018). Mitochondria: a master regulator in macrophage and T cell immunity. *Mitochondrion* 41, 45–50. <https://doi.org/10.1016/j.mito.2017.11.002>.
  42. Yang, S.K., Zhang, H.R., Shi, S.P., Zhu, Y.Q., Song, N., Dai, Q., Zhang, W., Gui, M., and Zhang, H. (2020). The role of mitochondria in systemic lupus erythematosus: a glimpse of various pathogenetic mechanisms. *Curr. Med. Chem.* 27, 3346–3361. <https://doi.org/10.2174/0929867326666181126165139>.
  43. Caza, T.N., Fernandez, D.R., Talaber, G., Oaks, Z., Haas, M., Madaio, M.P., Lai, Z.-w., Miklossy, G., Singh, R.R., Chudakov, D.M., et al. (2014). HRES-1/Rab4-mediated depletion of Drp1 impairs mitochondrial homeostasis and represents a target for treatment in SLE. *Ann. Rheum. Dis.* 73, 1888–1897. <https://doi.org/10.1136/annrheumdis-2013-203794>.
  44. Tomilov, A., Tomilova, N., Shan, Y., Hagopian, K., Bettaieb, A., Kim, K., Pellicci, P.G., Haj, F., Ramsey, J., and Cortopassi, G. (2016). p46Shc inhibits thiolase and lipid oxidation in mitochondria. *J. Biol. Chem.* 291, 12575–12585. <https://doi.org/10.1074/jbc.M115.695577>.
  45. Casals, N., Zammit, V., Herrero, L., Fadó, R., Rodríguez-Rodríguez, R., and Serra, D. (2016). Carnitine palmitoyltransferase 1C: from cognition to cancer. *Prog. Lipid Res.* 61, 134–148. <https://doi.org/10.1016/j.plipres.2015.11.004>.
  46. Franchina, D.G., Dostert, C., and Brenner, D. (2018). Reactive oxygen species: involvement

- in T cell signaling and metabolism. *Trends Immunol.* 39, 489–502. <https://doi.org/10.1016/j.it.2018.01.005>.
47. Perl, A. (2013). Oxidative stress in the pathology and treatment of systemic lupus erythematosus. *Nat. Rev. Rheumatol.* 9, 674–686. <https://doi.org/10.1038/nrrheum.2013.147>.
  48. Yao, Y., Chen, Z., Zhang, H., Chen, C., Zeng, M., Yunis, J., Wei, Y., Wan, Y., Wang, N., Zhou, M., et al. (2021). Selenium-GPX4 axis protects follicular helper T cells from ferroptosis. *Nat. Immunol.* 22, 1127–1139. <https://doi.org/10.1038/s41590-021-00996-0>.
  49. Bharath, L.P., Agrawal, M., McCambridge, G., Nicholas, D.A., Hasturk, H., Liu, J., Jiang, K., Liu, R., Guo, Z., Deeney, J., et al. (2020). Metformin enhances autophagy and normalizes mitochondrial function to alleviate aging-associated inflammation. *Cell Metabol.* 32, 44–55.e6. <https://doi.org/10.1016/j.cmet.2020.04.015>.
  50. Scarpulla, R.C., Vega, R.B., and Kelly, D.P. (2012). Transcriptional integration of mitochondrial biogenesis. *Trends Endocrinol. Metabol.* 23, 459–466. <https://doi.org/10.1016/j.tem.2012.06.006>.
  51. Gergely, P., Niland, B., Gonchoroff, N., Pullmann, R., Phillips, P.E., and Perl, A. (2002). Persistent mitochondrial hyperpolarization, increased reactive oxygen intermediate production, and cytoplasmic alkalinization characterize altered IL-10 signaling in patients with systemic lupus erythematosus. *J. Immunol.* 169, 1092–1101.
  52. Bailis, W., Shyer, J.A., Zhao, J., Canaveras, J.C.G., Al Khazal, F.J., Qu, R., Steach, H.R., Bielecki, P., Khan, O., Jackson, R., et al. (2019). Distinct modes of mitochondrial metabolism uncouple T cell differentiation and function. *Nature* 571, 403–407. <https://doi.org/10.1038/s41586-019-1311-3>.
  53. O’Sullivan, D., and Pearce, E.L. (2015). Targeting T cell metabolism for therapy. *Trends Immunol.* 36, 71–80. <https://doi.org/10.1016/j.it.2014.12.004>.
  54. Ma, E.H., Bantug, G., Griss, T., Condotta, S., Johnson, R.M., Samborska, B., Mainolfi, N., Suri, V., Guak, H., Balmer, M.L., et al. (2017). Serine is an essential metabolite for effector T cell expansion. *Cell Metabol.* 25, 345–357. <https://doi.org/10.1016/j.cmet.2016.12.011>.
  55. Lampropoulou, V., Sergushichev, A., Bambouskova, M., Nair, S., Vincent, E.E., Loginicheva, E., Cervantes-Barragan, L., Ma, X., Huang, S.C.C., Griss, T., et al. (2016). Itaconate links inhibition of succinate dehydrogenase with macrophage metabolic remodeling and regulation of inflammation. *Cell Metabol.* 24, 158–166. <https://doi.org/10.1016/j.cmet.2016.06.004>.
  56. Intlekofer, A.M., Dematteo, R.G., Venneti, S., Finley, L.W.S., Lu, C., Judkins, A.R., Rustenburg, A.S., Grinaway, P.B., Chodera, J.D., Cross, J.R., and Thompson, C.B. (2015). Hypoxia induces production of L-2-hydroxyglutarate. *Cell Metabol.* 22, 304–311. <https://doi.org/10.1016/j.cmet.2015.06.023>.
  57. Cisternas, P., Silva-Alvarez, C., Martínez, F., Fernández, E., Ferrada, L., Oyarce, K., Salazar, K., Bolaños, J.P., and Nualart, F. (2014). The oxidized form of vitamin C, dehydroascorbic acid, regulates neuronal energy metabolism. *J. Neurochem.* 129, 663–671. <https://doi.org/10.1111/jnc.12663>.
  58. Fu, G., Guy, C.S., Chapman, N.M., Palacios, G., Wei, J., Zhou, P., Long, L., Wang, Y.D., Qian, C., Dhungana, Y., et al. (2021). Metabolic control of T(FH) cells and humoral immunity by phosphatidylethanolamine. *Nature* 595, 724–729. <https://doi.org/10.1038/s41586-021-03692-z>.
  59. Jury, E.C., Flores-Borja, F., and Kabouridis, P.S. (2007). Lipid rafts in T cell signalling and disease. *Semin. Cell Dev. Biol.* 18, 608–615. <https://doi.org/10.1016/j.semcdb.2007.08.002>.
  60. Howie, D., Cobbold, S.P., Adams, E., Ten Bokum, A., Necula, A.S., Zhang, W., Huang, H., Roberts, D.J., Thomas, B., Hester, S.S., et al. (2017). Foxp3 drives oxidative phosphorylation and protection from lipotoxicity. *JCI Insight* 2, e89160. <https://doi.org/10.1172/jci.insight.89160>.
  61. Walker, L.S.K. (2022). The link between circulating follicular helper T cells and autoimmunity. *Nat. Rev. Immunol.* 22, 567–575. <https://doi.org/10.1038/s41577-022-00693-5>.
  62. Choi, J., Diao, H., Faliti, C.E., Truong, J., Rossi, M., Bélanger, S., Yu, B., Goldrath, A.W., Pipkin, M.E., and Crotty, S. (2020). Bcl-6 is the nexus transcription factor of T follicular helper cells via repressor-of-repressor circuits. *Nat. Immunol.* 21, 777–789. <https://doi.org/10.1038/s41590-020-0706-5>.
  63. Kurata, I., Matsumoto, I., and Sumida, T. (2021). T follicular helper cell subsets: a potential key player in autoimmunity. *Immunol. Med.* 44, 1–9. <https://doi.org/10.1080/25785826.2020.1776079>.
  64. Ochiai, K., Maienschein-Cline, M., Simonetti, G., Chen, J., Rosenthal, R., Brink, R., Chong, A.S., Klein, U., Dinner, A.R., Singh, H., and Sciammas, R. (2013). Transcriptional regulation of germinal center B and plasma cell fates by dynamical control of IRF4. *Immunity* 38, 918–929. <https://doi.org/10.1016/j.immuni.2013.04.009>.
  65. Bartleson, J.M., Viehmann Milam, A.A., Donermeyer, D.L., Horvath, S., Xia, Y., Egawa, T., and Allen, P.M. (2020). Strength of tonic T cell receptor signaling instructs T follicular helper cell-fate decisions. *Nat. Immunol.* 21, 1384–1396. <https://doi.org/10.1038/s41590-020-0781-7>.
  66. Biram, A., Davidzohn, N., and Shulman, Z. (2019). T cell interactions with B cells during germinal center formation, a three-step model. *Immunol. Rev.* 288, 37–48. <https://doi.org/10.1111/immr.12737>.
  67. Zhong, M.C., Lu, Y., Qian, J., Zhu, Y., Dong, L., Zahn, A., Di Noia, J.M., Karo-Atar, D., King, I.L., and Veillette, A. (2021). SLAM family receptors control pro-survival effectors in germinal center B cells to promote humoral immunity. *J. Exp. Med.* 218, e20200756. <https://doi.org/10.1084/jem.20200756>.
  68. Zhou, X., Qi, H., Li, M., Li, Y., Zhu, X., Amin, S., Alexander, M., Diadhiou, C., Davidson, A., and Zeng, H. (2023). mTORC2 contributes to systemic autoimmunity. *Immunology* 168, 554–568. <https://doi.org/10.1111/imm.13594>.
  69. Oaks, Z., Winans, T., Huang, N., Banki, K., and Perl, A. (2016). Activation of the mechanistic target of rapamycin in SLE: explosion of evidence in the last five years. *Curr. Rheumatol. Rep.* 18, 73. <https://doi.org/10.1007/s11926-016-0622-8>.
  70. Caza, T.N., Talaber, G., and Perl, A. (2012). Metabolic regulation of organelle homeostasis in lupus T cells. *Clin. Immunol.* 144, 200–213. <https://doi.org/10.1016/j.clim.2012.07.001>.
  71. Perry, D.J., Yin, Y., Telarico, T., Baker, H.V., Dozmorov, I., Perl, A., and Morel, L. (2012). Murine lupus susceptibility locus Sle1c2 mediates CD4+ T cell activation and maps to estrogen-related receptor gamma. *J. Immunol.* 189, 793–803. <https://doi.org/10.4049/jimmunol.1200411>.
  72. Li, W., Gong, M., Park, Y.P., Elshikha, A.S., Choi, S.C., Brown, J., Kanda, N., Yeh, W.I., Peters, L., Titov, A.A., et al. (2021). Lupus susceptibility gene Esrrg modulates regulatory T cells through mitochondrial metabolism. *JCI Insight* 6, e143540. <https://doi.org/10.1172/jci.insight.143540>.
  73. Lai, Z.-W., Hanczko, R., Bonilla, E., Caza, T.N., Clair, B., Bartos, A., Miklossy, G., Jimah, J., Doherty, E., Tily, H., et al. (2012). N-acetylcysteine reduces disease activity by blocking mTOR in T cells of lupus patients. *Arthritis Rheum.* 64, 2937–2946.
  74. Perl, A. (2016). Activation of mTOR (mechanistic target of rapamycin) in rheumatic diseases. *Nat. Rev. Rheumatol.* 12, 169–182. <https://doi.org/10.1038/nrrheum.2015.172>.
  75. Rai, P., Janardhan, K.S., Meacham, J., Madenspacher, J.H., Lin, W.C., Karmaus, P.W.F., Martinez, J., Li, Q.Z., Yan, M., Zeng, J., et al. (2021). IRGM1 links mitochondrial quality control to autoimmunity. *Nat. Immunol.* 22, 312–321. <https://doi.org/10.1038/s41590-020-00859-0>.
  76. Pantic, B., Ives, D., Mennuni, M., Perez-Rodriguez, D., Fernandez-Pelayo, U., Lopez de Arbina, A., Muñoz-Oreja, M., Villar-Fernandez, M., Dang, T.M.J., Vergani, L., et al. (2021). 2-Deoxy-D-glucose couples mitochondrial DNA replication with mitochondrial fitness and promotes the selection of wild-type over mutant mitochondrial DNA. *Nat. Commun.* 12, 6997. <https://doi.org/10.1038/s41467-021-26829-0>.
  77. Kono, M., Yoshida, N., and Tsokos, G.C. (2021). Amino acid metabolism in lupus. *Front. Immunol.* 12, 623844. <https://doi.org/10.3389/fimmu.2021.623844>.
  78. Spinelli, J.B., Yoon, H., Ringel, A.E., Jeanfavre, S., Clish, C.B., and Haigis, M.C. (2017). Metabolic recycling of ammonia via glutamate dehydrogenase supports breast

- cancer biomass. *Science* 358, 941–946. <https://doi.org/10.1126/science.aam9305>.
79. Caielli, S., Veiga, D.T., Balasubramanian, P., Athale, S., Domic, B., Murat, E., Bancheureau, R., Xu, Z., Chandra, M., Chung, C.H., et al. (2019). A CD4(+) T cell population expanded in lupus blood provides B cell help through interleukin-10 and succinate. *Nat. Med.* 25, 75–81. <https://doi.org/10.1038/s41591-018-0254-9>.
80. Saraiva, A.L., Veras, F.P., Peres, R.S., Talbot, J., Lima, K.A., Luiz, J.P., Carballido, J.M., Cunha, T.M., Cunha, F.Q., Ryffel, B., and Alves-Filho, J.C. (2018). Succinate receptor deficiency attenuates arthritis by reducing dendritic cell traffic and expansion of Th17 cells in the lymph nodes. *Faseb. J.* 32, 6550–6558. <https://doi.org/10.1096/fj.201800285>.
81. Lin, J., Yu, Y., Ma, J., Ren, C., and Chen, W. (2019). PD-1+CXCR5-CD4+T cells are correlated with the severity of systemic lupus erythematosus. *Rheumatology* 58, 2188–2192. <https://doi.org/10.1093/rheumatology/kez228>.
82. Le Coz, C., Joubin, A., Pasquali, J.-L., Korganow, A.-S., Dumortier, H., and Monneaux, F. (2013). Circulating T<sub>FH</sub> subset distribution is strongly affected in lupus patients with an active disease. *PLoS One* 8, e75319. <https://doi.org/10.1371/journal.pone.0075319>.
83. Han, L., Yang, X., Yu, Y., Wan, W., Lv, L., and Zou, H. (2019). Associations of circulating CXCR3(-)PD-1(+)/CD4(+)T cells with disease activity of systemic lupus erythematosus. *Mod. Rheumatol.* 29, 461–469. <https://doi.org/10.1080/14397595.2018.1469581>.
84. Odegard, J.M., Marks, B.R., DiPlacido, L.D., Poholek, A.C., Kono, D.H., Dong, C., Flavell, R.A., and Craft, J. (2008). ICOS-dependent extrafollicular helper T cells elicit IgG production via IL-21 in systemic autoimmunity. *J. Exp. Med.* 205, 2873–2886. <https://doi.org/10.1084/jem.20080840>.
85. Dobin, A., Davis, C.A., Schlesinger, F., Drenkow, J., Zaleski, C., Jha, S., Batut, P., Chaisson, M., and Gingeras, T.R. (2013). STAR: ultrafast universal RNA-seq aligner. *Bioinformatics* 29, 15–21. <https://doi.org/10.1093/bioinformatics/bts635>.
86. Liao, Y., Smyth, G.K., and Shi, W. (2014). featureCounts: an efficient general purpose program for assigning sequence reads to genomic features. *Bioinformatics* 30, 923–930. <https://doi.org/10.1093/bioinformatics/btt656>.
87. Love, M.I., Huber, W., and Anders, S. (2014). Moderated estimation of fold change and dispersion for RNA-seq data with DESeq2. *Genome Biol.* 15, 550. <https://doi.org/10.1186/s13059-014-0550-8>.
88. Subramanian, A., Tamayo, P., Mootha, V.K., Mukherjee, S., Ebert, B.L., Gillette, M.A., Paulovich, A., Pomeroy, S.L., Golub, T.R., Lander, E.S., and Mesirov, J.P. (2005). Gene set enrichment analysis: a knowledge-based approach for interpreting genome-wide expression profiles. *Proc. Natl. Acad. Sci. USA* 102, 15545–15550. <https://doi.org/10.1073/pnas.0506580102>.
89. Liberzon, A., Birger, C., Thorvaldsdóttir, H., Ghandi, M., Mesirov, J.P., and Tamayo, P. (2015). The molecular signatures database (MSigDB) hallmark gene set collection. *Cell Syst.* 1, 417–425. <https://doi.org/10.1016/j.cels.2015.12.004>.
90. Zou, X., Choi, S.C., Zeumer-Spataro, L., Scindia, Y., Moser, E.K., and Morel, L. (2022). Metabolic regulation of follicular helper T cell differentiation in a mouse model of lupus. *Immunol. Lett.* 247, 13–21. <https://doi.org/10.1016/j.imlet.2022.03.008>.
91. Kind, T., Wohlgemuth, G., Lee, D.Y., Lu, Y., Palazoglu, M., Shahbaz, S., and Fiehn, O. (2009). FiehnLib: mass spectral and retention index libraries for metabolomics based on quadrupole and time-of-flight gas chromatography/mass spectrometry. *Anal. Chem.* 81, 10038–10048. <https://doi.org/10.1021/ac9019522>.
92. Lai, Z., Tsugawa, H., Wohlgemuth, G., Mehta, S., Mueller, M., Zheng, Y., Ogiwara, A., Meissen, J., Showalter, M., Takeuchi, K., et al. (2018). Identifying metabolites by integrating metabolome databases with mass spectrometry cheminformatics. *Nat. Methods* 15, 53–56. <https://doi.org/10.1038/nmeth.4512>.
93. Chong, J., Wishart, D.S., and Xia, J. (2019). Using MetaboAnalyst 4.0 for comprehensive and integrative metabolomics data analysis. *Curr. Protoc. Bioinformatics* 68, e86. <https://doi.org/10.1002/cpbi.86>.
94. Kandasamy, P., Gyimesi, G., Kanai, Y., and Hediger, M.A. (2018). Amino acid transporters revisited: new views in health and disease. *Trends Biochem. Sci.* 43, 752–789. <https://doi.org/10.1016/j.tibs.2018.05.003>.

**STAR★METHODS**

**KEY RESOURCES TABLE**

REAGENT or RESOURCE	SOURCE	IDENTIFIER
<i>Antibodies</i>		
BCL-2 PE/Cy7	BioLegend	RRID: AB_2565247
BCL-6 AF647	BD Biosciences	RRID: AB_10898007
CD3e	BD Biosciences	RRID: AB_394590
CD4 AF700	Thermo Fisher	RRID: AB_493999
CD4 APC	BioLegend	RRID: AB_312719
CD4 eF450	Thermo Fisher	RRID: AB_10718983
CD4 FITC	BD Biosciences	RRID: AB_394583
CD16/CD32	BD Biosciences	RRID: AB_394655
CD28 biotin	Thermo Fisher	RRID; AB_466411
CD28	BD Biosciences	RRID: AB_394763
CD44 PE	BioLegend	RRID: AB_312959
CD48 FITC	Thermo Fisher	RRID: AB_465076
CD69PE/Cy7	BioLegend	RRID: AB_493564
CD84 PE	BioLegend	RRID: AB_2074757
CD95 biotin	BD Biosciences	RRID: AB_395328
CD122 PE	Thermo Fisher	RRID: AB_465832
CD134 APC	Thermo Fisher	RRID: AB_10717260
CD150 PE/Cy7	BioLegend	RRID: AB_439796
CD152 APC	BioLegend	RRID: AB_2087653
CD153 biotin	Thermo Fisher	RRID: AB_466622
CD162 AF647	BD Biosciences	RRID: AB_2737807
CD183 BV421	BioLegend	RRID: AB_2563100
CD185	BD Biosciences	RRID: AB_394302
CD197 PE	BioLegend	RRID: AB_389357
CD229 PE	BioLegend	RRID: AB_2137958
CD244.2 PE/Cy7	Thermo Fisher	RRID: AB_257343
CD267 APC	Thermo Fisher	RRID: AB_842759
CD278 PE	BD Biosciences	RRID: AB_394349
CD279 eF450	Thermo Fisher	RRID: AB_11150068
CD279 PE/Cy7	Thermo Fisher	RRID: AB_10853805
GATA3 PE/Cy7	Thermo Fisher	RRID: AB_2573568
IFN-γ Pacific blues	BioLegend	RRID: AB_893526
IFN-γ	Bio X cell	RRID: AB_1107694
IFN-γR1	Thermo Fisher	RRID: AB_2573097
IL-10R PE	BioLegend	RRID: AB_313518
IL-21R APC	BioLegend	RRID: AB_2295868
IL-23R PE	BioLegend	RRID: AB_2572188
IL-2	BioLegend	RRID: AB_315292
IL-4	Bio X cell	RRID: AB_1107707
IRF4 eF660	Thermo Fisher	RRID: AB_2574393
Ly108 PE	Thermo Fisher	RRID: AB_763616

(Continued on next page)

**Continued**

REAGENT or RESOURCE	SOURCE	IDENTIFIER
Nur77 PE	Thermo Fisher	RRID: AB_1257210
p4E-BP1 AF647	Cell Signaling	RRID: AB_2097838
pAKT PE/Cy7	Thermo Fisher	RRID: AB_2688172
pS6 Pacific blue	Cell Signaling	RRID: AB_2797646
RORyT BV421	BD Biosciences	RRID: AB_2687545
T-bet eF450	Thermo Fisher	RRID: AB_2784726
TGF- $\beta$	R&D Systems	RRID: AB_357931
Anti-rabbit IgG HRP	Cell Signaling	RRID: AB_2099233
Anti-mouse IgG HRP	Cell Signaling	RRID: AB_330924
H3K36me2 Ab	Cell Signaling	RRID: AB_1030983
Histone 3 Ab	Cell Signaling	RRID: AB_2756816

Chemicals, peptides, and recombinant proteins

Fixable viability dye	Thermo Fisher	65-0865
MitoSOX™ Red	Thermo Fisher	M36008
CM-H2DCFDA	Thermo Fisher	C6827
MitoTracker® Red CMXRos	Thermo Fisher	M7512
MitoTracker™ Deep Red	Thermo Fisher	M22426
2-NBDG	Thermo Fisher	N13195
BODIPY	Thermo Fisher	D3823
Duramycin-LC	Molecular Targeting Technologies	D-1003
Streptavidin PE/Cy7	BD Biosciences	557598
Streptavidin BV650	BioLegend	405231
Streptavidin PerCP	BD Biosciences	554064
dsDNA	Sigma	D8515
p-nitrophenol phosphate (PNPP) substrate	Thermo Fisher	34045
4 - 20% SDS-PAGE gels	Bio-Rad	4561094
Western ECL substrate	Cell Signaling	6883S
AMPure XP beads	Beckman Coulter	A63880
Restore™ Western Blot Stripping Buffer	Thermo Fisher	21059
Foxp3 / Transcription Factor Staining Buffer Set	Thermo Fisher	00-5523-00
cell signaling lysis buffer	Sigma	43-040
protease inhibitor cocktail	Sigma	S8820-20
SYBR® Green Supermix	Bio-Rad	1725271
RPMI-1640	Corning	10-040-CV
IL-6	Shenandoah Biotech	200-02
IL-21	Pepro Tech	210-21
Activin A	Thermo Fisher	PHC9564

Critical commercial assays

RNeasy Kit	Qiagen	74004
TruSeq Stranded RNA Sample Preparation Kit	Illumina	20020597
PicoGreen assay	Thermo Fisher	P7589
CD4 T Cell Isolation Kit	Miltenyi Biotec	<a href="#">130-104-454</a>
Naïve CD4 T Cell Isolation Kit	Miltenyi Biotec	<a href="#">130-104-453</a>
BCA protein assay kit	Pierce	23225
Impromptu-II™ Reverse Transcription System	Promega	A3800

(Continued on next page)

**Continued**

REAGENT or RESOURCE	SOURCE	IDENTIFIER
<b>Deposited data</b>		
Raw RNA-seq data	GEO	GSE 157648
Other raw and processed data	GitHub	<a href="https://github.com/gmhhope/TC_TFH_omics_analysis/">https://github.com/gmhhope/TC_TFH_omics_analysis/</a> .
Analysis workflows		<a href="https://github.com/gmhhope/TC_TFH_omics_analysis/">https://github.com/gmhhope/TC_TFH_omics_analysis/</a> .
<b>Experimental models: Organisms/strains</b>		
B6.NZM-Sle1 <sup>NZM2410/Aeg</sup> Sle2 <sup>NZM2410/Aeg</sup> Sle3 <sup>NZM2410/Aeg</sup> /LmoJ (TC) female mice	In house and Jackson laboratories	# 007228
C57BL6/J female mice	Jackson laboratories	#000664
<b>Oligonucleotides</b>		
Smyd2 F	N/A	F: 5'-AAGGATTGTCAAAATGTGGACGG-3'
Smyd2 R	N/A	R: 5'-ATGGAGGAGCATTCCAGCTTG-3'
Hsp90 F	N/A	F: 5'-GTCCGCCGTGTGTTTCATCAT-3'
Hsp90 R	N/A	R: 5'-GCACTTCTTGACGATGTTCTTGC-3'
<b>Software and algorithms</b>		
FlowJo V10	Tree Star	<a href="https://www.flowjo.com/solutions/flowjo/downloads">https://www.flowjo.com/solutions/flowjo/downloads</a>
Prism 9.0	Graphpad	<a href="https://www.graphpad.com/scientific-software/prism/">https://www.graphpad.com/scientific-software/prism/</a>
ImageJ	NIH	<a href="https://imagej.nih.gov/ij/">https://imagej.nih.gov/ij/</a>
STAR aligner v2.7 <sup>85</sup>	N/A	<a href="https://github.com/alexdobin/STAR">https://github.com/alexdobin/STAR</a>
FeatureCounts (v2.0)	N/A	<a href="https://subread.sourceforge.net/featureCounts.html">https://subread.sourceforge.net/featureCounts.html</a>
DESeq	N/A	<a href="https://bioconductor.org/packages/release/bioc/html/DESeq2.html">https://bioconductor.org/packages/release/bioc/html/DESeq2.html</a>
pheatmap R function (version 1.0.12)	N/A	<a href="https://www.rdocumentation.org/packages/pheatmap/versions/1.0.12/topics/pheatmap">https://www.rdocumentation.org/packages/pheatmap/versions/1.0.12/topics/pheatmap</a>
Matplotlib-Venn (Version 0.11.5)	N/A	<a href="https://packages.ubuntu.com/bionic/python-matplotlib-venn">https://packages.ubuntu.com/bionic/python-matplotlib-venn</a>
javaGSEA (v3.0)	N/A	<a href="https://www.gsea-msigdb.org/gsea/index.jsp">https://www.gsea-msigdb.org/gsea/index.jsp</a>
Molecular Signature Database (MSigDB v5.2)	N/A	<a href="https://www.gsea-msigdb.org/gsea/msigdb/">https://www.gsea-msigdb.org/gsea/msigdb/</a>
R function Dotplot in Lattice package (version 0.3-1)	N/A	<a href="https://www.rdocumentation.org/packages/lattice/versions/0.3-1/topics/dotplot">https://www.rdocumentation.org/packages/lattice/versions/0.3-1/topics/dotplot</a>
Metamorph software	Molecular Devices	<a href="https://www.moleculardevices.com/products/cellular-imaging-systems/acquisition-and-analysis-software/metamorph-microscopy">https://www.moleculardevices.com/products/cellular-imaging-systems/acquisition-and-analysis-software/metamorph-microscopy</a>
<b>Others</b>		
ACE 18-PFP 100 x 2.1 mm, 2 μm column	Mac-Mod Analytical	N/A
LSRFortessa	BD Biosciences	N/A
FACS Aria III	BD Biosciences	N/A

**RESOURCE AVAILABILITY**

This study did not generate new unique reagents.

**Lead contact**

Further information and requests for resources and reagents should be directed to and will be fulfilled by the lead contact, Dr. Laurence Morel ([morel@uthscsa.edu](mailto:morel@uthscsa.edu)).

### Data and code availability

This paper does not report original code. Raw RNA-seq data are publicly available in GEO under the entry: GSE 157648. All the other raw and processed data including Metabolomic dataset and experimental dataset are stored in the Github repository: [https://github.com/gmhhope/TC\\_TFH\\_omics\\_analysis/](https://github.com/gmhhope/TC_TFH_omics_analysis/). The analysis workflows are publicly available in the Github repository: [https://github.com/gmhhope/TC\\_TFH\\_omics\\_analysis/](https://github.com/gmhhope/TC_TFH_omics_analysis/). Any additional information required to reanalyze the data reported in this paper is available from the [lead contact](#) upon request.

### EXPERIMENTAL MODEL AND SUBJECT DETAILS

The B6.NZM-Sle1<sup>NZM2410/Aeg</sup>Sle2<sup>NZM2410/Aeg</sup>Sle3<sup>NZM2410/Aeg</sup>/LmoJ (TC) congenic mice have been previously described.<sup>9</sup> C57BL/6J (B6) were originally purchased from the Jackson Laboratories. B6 and TC mice were bred and maintained at the University of Florida in specific pathogen-free conditions. AntidsDNA IgG positive female TC mice between 7- and 9-months old and age-matched B6 controls were used. Representative values of the frequency of CD4<sup>+</sup> T cells in these mice are shown in [Table S1](#). All procedures were performed under protocols approved by the Institutional Animal Care and Use Committees of the University of Florida and Vanderbilt University.

### METHOD DETAILS

#### Flow cytometry and cell sorting

Single-cell suspensions were prepared from spleens using standard procedures. After red blood cell lysis, cells were stained in FACS staining buffer (2.5% FBS, 0.05% sodium azide in PBS). Fluorochrome-conjugated antibodies (Abs) used for flow cytometry are listed in the [key resources table](#). Tfh cells were sorted as CD44<sup>+</sup>PSGL-1<sup>lo</sup>PD-1<sup>+</sup>CD4<sup>+</sup> (ref 22) for RNASeq, metabolomic and Western blot analyses. Tfh cells were gated as PD1<sup>+</sup>BCL-6<sup>+</sup>CXCR5<sup>+</sup>FOXP3<sup>+</sup>CD4<sup>+</sup> cells in FACS analyses with CXCR5 stained in a three-step process using purified anti-CXCR5 followed by biotinylated anti-rat IgG then PerCP-labeled streptavidin.<sup>25</sup> For intracellular staining, cells were fixed and permeabilized with FOXP3 staining buffer. Dead cells were excluded with fixable viability dye. Mitochondrial ROS was measured by MitoSOX<sup>TM</sup> Red and cellular ROS was measured with 2',7'-dichlorodihydrofluorescein diacetate (H2DCFDA). Mitochondrial mass and membrane potential were assessed with MitoTracker<sup>®</sup> Red CMXRos and MitoTracker<sup>TM</sup> Deep Red. To measure glucose or lipid uptake, total splenocytes (1 - 2 × 10<sup>6</sup>) were stained with Tfh-cell-gating fluorescence-conjugated Abs (CD4, PD-1, CXCR5 and BCL-6) for 30 min on ice and incubated with 20 mM 2-N-(7-nitrobenz-2-oxa-1,3-diazol-4-yl) amino-2-deoxyglucose (2-NBDG) or 2 mM BODIPY for 20 min at 37°C, respectively. Duramycin-LC-Biotin was used for measuring phosphoethanolamine (PE) on cell surface or intracellularly following staining with fluorescence-conjugated streptavidin. Data were collected on LSRFortessa and analyzed with FlowJo software. Tfh cells defined as CD4<sup>+</sup>CD44<sup>+</sup>PSGL-1<sup>lo</sup>-PD-1<sup>+</sup> and Tn cells defined as CD4<sup>+</sup>CD44<sup>-</sup> were sorted on a FACSAria III high-speed cell sorter from CD4<sup>+</sup> T cells purified by negative selection with magnetic beads ([Figure S1](#)).

#### RNA sequencing

RNA was extracted from FACS-sorted Tfh and Tn cells using the RNeasy Kit. RNA-seq libraries were prepared with the TruSeq Stranded RNA Sample Preparation Kit and the quality was verified with the Agilent Bioanalyzer 2100. The amplified libraries were size-selected using AMPure XP beads and quantified with the PicoGreen assay. Sequencing was performed on an Illumina Novaseq 6000 at the UF Interdisciplinary Center for Biotechnology Research (ICBR). Alignment of RNA-seq reads were mapped to the mm10 *Mus musculus* genome with STAR aligner v2.7.<sup>85</sup> FeatureCounts (v2.0) was used to calculate gene counts for each sample.<sup>86</sup> Significantly differentially expressed genes (DEG, FDR P < 0.05) were identified by DESeq2.<sup>87</sup> To understand the global distribution of DEG among the 4 groups, principal component analysis and Euclidean distance matrix were generated with functions embedded in DESeq2. Microarray and Nanostring datasets previously described<sup>25</sup> were reanalyzed to compare with the RNA-seq data generated in this study. To globally compare results generated from these different platforms or different comparisons, Pearson correlation analyses were computed on the indicated list of Wald-statistics.<sup>25</sup> Regularized-log-transformation of count data or log2-transformed fold changes were performed for heatmap plotting using the pheatmap R function (version 1.0.12). Venn-diagrams were generated using the Python function Matplotlib-Venn (Version 0.11.5). Gene set enrichment analyses (GSEA) were performed in javaGSEA (v3.0) using rank-lists based on Wald-statistics, which were generated from the DESeq2 analysis.<sup>88</sup> GSEA analyses included the GO, KEGG and REACTOME databases. Specific gene sets used for analyses were retrieved

from the Molecular Signature Database (MSigDB v5.2).<sup>89</sup> For gene overlap analysis, significant overlaps with KEGG gene sets in MSigDB were computed on the MSigDB website (<https://www.gsea-msigdb.org/gsea/msigdb/annotate.jsp>) and were plotted using the R function Dotplot in Lattice package (version 0.3-1).

### Western blot and qRT-PCR analysis

Tn and T<sub>eff</sub> cells defined as CD62L<sup>+</sup>CD44<sup>+</sup> sorted from B6 or TC mice were lysed in cell signaling lysis buffer containing a protease inhibitor cocktail. After brief sonication, cells were incubated for 30 min on ice and centrifuged at 12,000 rpm for 20 min at 4°C to collect the soluble supernatant. Proteins in the cell lysates were quantified with the BCA protein assay kit. 30 µg of cell lysates were run on 4 - 20% SDS-PAGE gels and transferred to PVDF membranes. Membranes were blocked with 5% non-fat dry milk in Tris-buffered saline containing 0.1% Tween-20 for 1 h at room temperature, then incubated with a rabbit anti-H3K36me2 Ab overnight at 4°C. Membranes were then washed and incubated with horseradish peroxidase-conjugated secondary Ab for 1 h. Western ECL substrate was used to develop the immunoblot. After bound Abs were removed using Restore™ Western Blot Stripping Buffer, membranes were incubated with mouse anti-histone 3 Ab for normalization. Band intensity was calculated with Image J. cDNA was synthesized with the ImProm-II™ Reverse Transcription System. qRT-PCR analysis of *Smyd2* expression was performed with the SYBR® Green Supermix. Relative expression was calculated using 2<sup>ΔC<sub>q</sub></sup> values normalized to *Hsp90*.

### In vitro Tfh cells polarization

Tfh cells were generated from splenic naïve CD62L<sup>dim</sup>/CD4<sup>+</sup> T Cells purified by negative selection with magnetic beads as previously described.<sup>90</sup> Tn cells (1 × 10<sup>6</sup> per well) were activated in 24-well plates coated with 2 µg/ml anti-CD3e Ab with 1 ml of RPMI-1640 media (0.2 % glucose, 0.03% glutamine) supplemented with 10% FBS, 1 mM sodium pyruvate, 100 U/ml penicillin/streptomycin, and 10 mM HEPES with 1 µg/ml anti-CD28 Ab for 3 days. The Tfh polarizing cocktail contained 100 ng/ml IL-6, 50 ng/ml IL-21, 10 µg/ml anti-IL-2, 10 µg/ml anti-IFNγ, 10 µg/ml anti-IL-4, and 5 µg/ml anti-TGFβ Abs. Activin A was used at 100 ng/ml.

### Electron microscopy

CD44<sup>+</sup> (T<sub>eff</sub>) and CD44<sup>-</sup> (Tn) CD4<sup>+</sup> T cells isolated with magnetic beads were visualized on a Hitachi H-7000 TEM transmission electron microscope at the UF ICBR electron microscopy core. For each sample, measurements of mitochondria were performed at X 20,000 magnification using the Metamorph software.

### Metabolomic analyses

Sorted Tn and Tfh cells (0.5 – 1 × 10<sup>6</sup>) were analyzed at the UC Davis West Coast Metabolomics Center using untargeted metabolomics by gas chromatography-time of flight-mass spectrometry (GC-TOF-MS). A standard primary metabolite extraction protocol was applied, with 100 µl of 3:3:2 acetonitrile:isopropyl alcohol: water added to 0.5 µl cells, followed by centrifugation, decanting, desiccation and trimethylsilylation for GC-TOF-MS profiling using Fiehn laboratory standard operating procedures.<sup>91</sup> Identification of metabolite features was performed by comparison to the BinBase database<sup>92</sup> and their quantity normalized to the cell count in each sample. Cells from two cohorts of mice were processed and analyzed separately and recombined to obtain a data matrix with 303 metabolites including 110 unique structurally annotated compounds. Only annotated compound features (mTIC) were used for subsequent analyses. Data analysis was performed either in R version 3.5.3 using RStudio (Version 1.2.1335) or in Python version 3.6.5 using Jupyter Notebook (Version 5.5.0). The data matrix was normalized to average mTIC of the samples and log<sub>2</sub>-transformed. PCA analyses were performed on the annotated features using MetaboAnalyst 4.0.<sup>93</sup> Statistical analyses included one-way ANOVA and pair-wise Student's t test as indicated in the text using Python package SciPy (version 1.1.0). FDR adjusted p values were generated for the annotated features using Benjamini-Hochberg Procedure with R function p.adjust. The heatmap presentation of the hierarchical clustering analyses was performed using Python package Seaborn (version 0.10.1). Other heatmap presentations were performed in R function pheatmap (version 1.0.12). Pathway analyses were performed using enrichment analysis function in MetaboAnalyst 4.0. Only the pathways with adjusted p-values < 0.25 were showed in bubble plots. Both box plots and bubble plots highlighting individual metabolites and pathways were plotted using ggplot2 (version 3.3.0). The metabolomic data of *in-vitro* polarized Tfh and activated T cells from B6 mice has been previously published.<sup>23</sup> For the network analysis of the dynamics

of amino acids and their transporters, the network prototype was mainly constructed based on annotations of amino acid transporters.<sup>94</sup> The layout was configured in Cytoscape ([Cytoscape.org](https://cytoscape.org)).

### QUANTIFICATION AND STATISTICAL ANALYSIS

Differences between two groups are computed with unpaired *t* tests or Mann-Whitney *U* tests according to the normality of the data. Multiple comparisons among more than three groups were performed by one-way ANOVA with post-tests multiple comparisons. Statistical significances of differences from RNA-seq and metabolomic analyses are computed according to their unique context expanded within aforementioned methods. Unless specified, graphs show means and standard error of the mean (s.e.m.).